MICROCOPY RESOLUTION TEST CHART

NATIONAL BUREAU OF STANDARDS-1963-A

ETL-0398

Electronic feedback control of mass – spring systems

Qin Kong

University of Maryland
Department of Physics and Astronomy
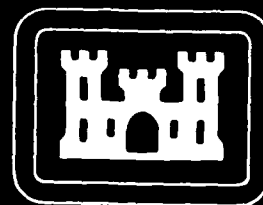College Park, Maryland 20742

September 1985

DTIC
ELECTE
OCT 2 9 1985
S   D
B

DTIC FILE COPY

REPORT DOCUMENTATION PAGE	READ INSTRUCTIONS BEFORE COMPLETING FORM

1. REPORT NUMBER	2. GOVT ACCESSION NO.	3. RECIPIENT'S CATALOG NUMBER
ETL–0398	AO-A160 691	

4. TITLE (and Subtitle)	5. TYPE OF REPORT & PERIOD COVERED
ELECTRONIC FEEDBACK CONTROL OF MASS–SPRING SYSTEMS	Special Report
	6. PERFORMING ORG. REPORT NUMBER

7. AUTHOR(s)	8. CONTRACT OR GRANT NUMBER(s)
Qin Kong	DACA72–84–C–0004

9. PERFORMING ORGANIZATION NAME AND ADDRESS	10. PROGRAM ELEMENT, PROJECT, TASK AREA & WORK UNIT NUMBERS
University of Maryland Department of Physics and Astronomy College Park, Maryland 20742	

11. CONTROLLING OFFICE NAME AND ADDRESS	12. REPORT DATE
U.S. Army Engineer Topographic Laboratories Fort Belvoir, Virginia 22060-5546	September 1985
	13. NUMBER OF PAGES
	102

14. MONITORING AGENCY NAME & ADDRESS(if different from Controlling Office)	15. SECURITY CLASS. (of this report)
	Unclassified
	15a. DECLASSIFICATION/DOWNGRADING SCHEDULE

16. DISTRIBUTION STATEMENT (of this Report)

Approved for public release; distribution is unlimited.

17. DISTRIBUTION STATEMENT (of the abstract entered in Block 20, if different from Report)

18. SUPPLEMENTARY NOTES

This report is a thesis submitted to the Graduate School of the University of Maryland in 1984. Another report prepared under the same contract is ETL–0397, Development of Electronic Control of Superconducting Gravity Gradiometer.

19. KEY WORDS (Continue on reverse side if necessary and identify by block number)

Ground motion isolation   Wide-band accelerometer
Josephson junction,
Mass-spring system
SQUID amplifier

20. ABSTRACT (Continue on reverse side if necessary and identify by block number)

This thesis develops an electronic system for the control of motion of different types of active springs, thus improving the performance of mass-spring systems. A mathematical analysis is carried out for various types of active springs. Also, this thesis discusses future design for improving the performance of these electronic circuits to achieve even better performance of mass-spring systems.

DD FORM 1473 EDITION OF 1 NOV 65 IS OBSOLETE

ABSTRACT

Title of Thesis: Electronic Feedback Control of

Mass-Spring Systems

Qin Kong, Master of Science, 1984

Thesis directed by: Robert W. Newcomb, Professor,

Department of Electrical Engineering

Ho Jung Paik, Associate Professor

Department of Physics and Astronomy

This thesis develops an electronic system for the control of motion of different types of active springs thus improving the performance of mass-spring systems. A mathematical analysis is carried out for various types of active springs. While keeping the mechanical springs and masses fixed, the stiffness and Q of the system are controlled electronically and made to depend on the gain of the electronic circuit.

A mass-spring system is a conventional mechanical structure which is used for many different purposes. It has been widely used in vibration isolation systems and sub-Hertz detectors. However, the conventional performance is limited by the size, the stiffness and Q of the spring.

In order to measure the system ground motion (noise) from 0-25 Hz, this thesis studies how to reduce $\frac{1}{f}$ noise and white noise of a preamplifier, how to pick a weak signal (ground motion) which is about $10^{-9} gHz^{-1/2}$, and how to make

sensitivity higher by impedence matching   Also it studies a special filter which uses frequency compensation to reduce noise.

The mechanical design is discussed as well. The results, which are valid for one dimensional motion only, include how to reduce the different modes of a spring.

The sensitivity of the electronic circuit is limited by the thermal noise.   Consequently, this thesis introduces a new low temperature device, the SQUID amplifier (Superconductiog QUantum Interference Device).   The SQUID amplifier works at temperatures under $4°K$ to reduce its thermal noise to zero.   So a superconducting mass-spring sensor with a SQUID amplifier can measure $10^{-13}gHz^{-1/2}$ of the ground motion.   The new sensor has very high sensitivity.   Therefore, a special cold damping circuit which lowers the amplitude of the resonance peak of the mass-spring system is necessary.

This thesis analyses and demonstrates two different ways to reduce the Q of the mass-spring system; these are the electromechanical and the electrical damping methods, The advantages and disadvantages of these damping methods are pointed out.

Also, this thesis discusses future design for improving the performance of these electronic circuits to achieve even better performance of mass-spring systems.

PREFACE

This document was prepared under contract DACA72-84-C-0004 for the U.S. Army Engineer Topographic Laboratories, Fort Belvoir, Virginia. The Contracting Officer's Technical Representative was Dr. Hans G. Baussus Von Luetzow.

i

ACKNOWLEDGEMENT

TABLE OF CONTENTS

LIST OF FIGURES

vii

INTRODUCTION

Mass-spring systems are widely used in Sub-Hertz frequency detectors and ground vibration isolations [Weinstoch,1968]. They are not only used in room temperature systems but also in low temperature systems.

In the ground vibration isolation system, air tables which are supported by an air bellows are commercially available.They can isolate the vibration when the frequency is greater then 4 Hz. The air table can satisfy most system needs to some degree, especially for a very large mass. However, it cannot isolate a frequency of the ground vibration which is higher than 4 Hz, because the rubber barry is not elastic enough. If we use a metal or rubber band spring instead of the air bellow, the resonant frequency can be very low. In other words the cut off frequency can be very much lowered over that obtainable with air tables. However, it is limited by the size of the spring. For instance, if the resonant frequency is at 2 Hz, the spring will be stretched about 6 cm, if the resonant frequency is at 0.2 Hz, the spring will be stretched about 6 m; this means it is not practical to make this latter kind of system.

The development of an active spring, the so-called super-spring, is one of the subjects of this thesis. It is a new mass-spring system in which the spring is short, but the spring has a very low resonant frequency which is controlled by an electronic circuit. Therefore the active

mass-spring system can isolate most vibrations from ground to platform (mass). In order to isolate the ground noise by an active mass-spring system, we have to measure the ground noise first. Control of white noise, $\frac{1}{f}$ noise, and sensitivity are difficult problems for electronic circuit design; these subjects will be discussed in Chapter 2 in detail.

Another subject of this thesis is to improve the performance of a superconducting sub-Hertz detector or accelerometer. A schematic illustration of a superconducting accelerometer is presented in Fig.1. Coils L_1 and L_2 form a superconducting loop which contains a persistant current I_0. L_2 is located very close to the superconducting proof mass. The proof mass will respond to an externally applied force with a displacement between the proof mass and L_1. Due to the Meissner effect [Paik,1974], this motion will modulate the inductance of L_1. Consequently, since the flux Φ in the superconducting loop is quantized, the flux change in L_1 must be compensated for by an equivalent flux change in L_2. Then by coupling L_2 to the input of a SQUID, very small accelerations can be detected [Moody,1983]. In order to reduce the noise of the accelerometer and keep it superconducting, the accelerometer best works in a vacuum at a low tempreture ($4\overset{\circ}{}K$). Therefore, the system has very high Q (50×10^3). The peak of its resonance will be very large to the point where it will saturate the SQUID amplifier which has very high

ACCELEROMETER HOUSE
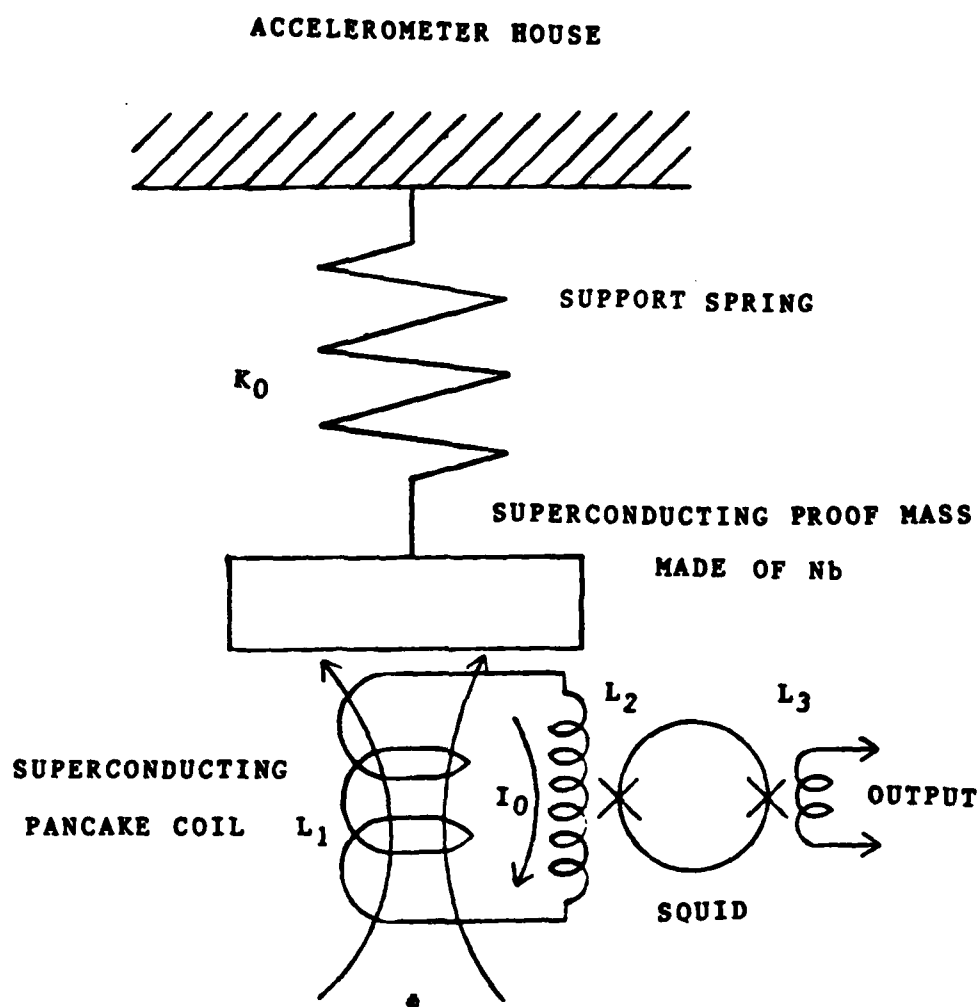
Fig.1. A Schematic of a Superconducting
Accelerometer

sensitivity. This shows that reduction of Q is necessary in a superconducting accelerometer. Two different ways to reduce Q of an accelerometer are presented in this thesis. One way is called electromechancial cold damping; it feeds back an additional force to the accelerometer to cancel the resonance peak. The other way is called electrical cold damping for which feed back is achieved via an electrical resistor from the accelerometer; this reduces the Q of the accelerometer because an accelerometer can be equivalent to an LRC circuit and the Q of the circuit is dependent on the total resistence in the circuit (which is $R+R_e$ where R_e is introduced by a control circuit).

In Chapter 1 of this thesis, a theory of a wideband supersprings is developed.

In Chapter 2, an electrical control circuit is designed to make a wideband superspring. The new circuit includes a displacement sensor made of four variable capacitors, a matching transformer, an analog switch demodulator, a power voltage-current converter and a compensation network.

In Chapter 3, the mechanical part of the superspring is designed. Some new ways to control modes of the spring are developed.

In Chapter 4, the test results of the superspring are discussed and agree with the theoretical value from the Chapter 1.

In Chapter 5, the different way to reduce the Q of a superconducting accelerometer is discussed. An

electromechanical cold damping method is developed. The test results are studied.

Chapter 6 discusses the future design and the appendix gives some background analysis and introduces a SQUID amplifier.

PART I

A MASS-SPRING SYSTEM AT ROOM TEMPERATURE

CHAPTER 1

THE WIDE BAND SUPERSPRING---AN ACTIVE SINGLE

MASS-SPRING LOW-PASS FILTER FOR GROUND MOTION ISOLATION

A wideband active mass-spring low pass filter, the so-
called wideband super-spring, for ground motion isolation
has been developed; the characteristic and realization of
the superspring will be studied in detail in this chapter.

Several people have studied the mass-spring noise
isolation system [Linsay,1982] [Rinker III,1983].   The
method that they used is represented in appendices A and
B.   The equations (B.7), (B.8) and (B.9) give the isolation
characteristics of their system.   The major disadventage is
that these systems only have very good isolation in a small
frequency range.   In order to improve these active spring-
mass noise isolation systems, a new wide band active mass-
spring noise isolation system, which can isolate all the
noise frequency which is higher than the resonance of this
system, will be analysed in the next sections.

1.1 Motion of a Single Mass-Spring System

The structure of a single mass-spring system is shown
in Fig.1.1 where k_1 is the spring constant; b_1 is the
damping factor of the spring; x_1 and x_2 are the absolute
displacement and f_b is an additional driving force coming
from a control system.   The following equations describe the
motion of this system.   By Newton's law, we get, on omitting
the driving force f_b for the time being,
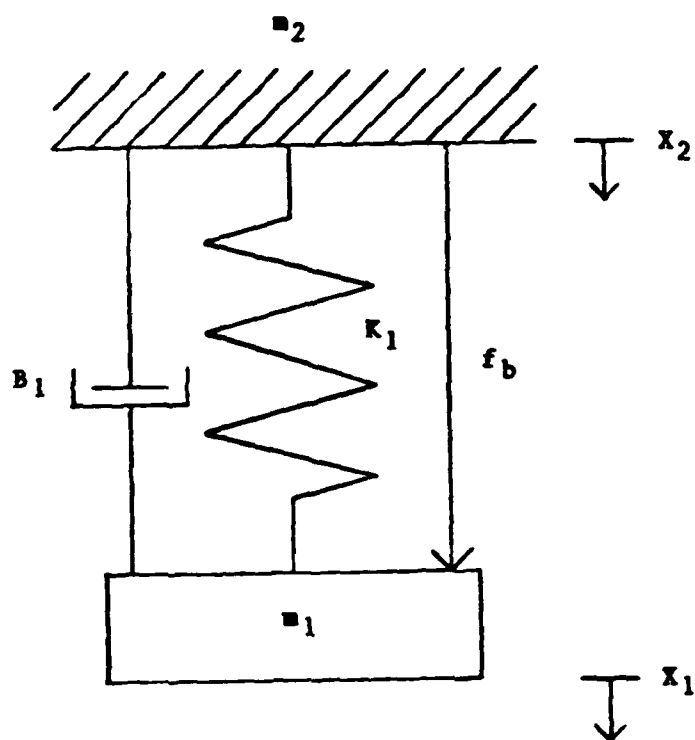
Fig.1.1. A Schematic of a Single Mass-Spring System.

$$\ddot{X}_1 m_1 + (\dot{X}_1 - \dot{X}_2)B_1 + K_1(X_1 - X_2) = 0 \tag{1.1}$$

or in the Laplace transform S domain,

$$m_1 X_1 S^2 + B_1(X_1 - X_2)S + K_1(X_1 - X_2) = 0 \tag{1.2}$$

and

$$X_1 = \frac{(\frac{B_1}{m_1}S + \frac{K_1}{m_1})}{S^2 + \frac{B_1}{m_1}S + \frac{K_1}{m_1}} X_2 \quad . \tag{1.3}$$

The equation (1.3) gives a low-pass filter characteristic from motion of m_2 to motion of m_1. The acceleration of m_1 and m_2 in terms of $(X_2 - X_1)$ are given by equation (A.6) and (A.11). Let us rewrite the equation (A.11) here

$$X_2 - X_1 = \frac{S^2 X_1}{\frac{B_1}{m_1}S + \frac{K_1}{m_1}} \quad . \tag{1.4}$$

This equation shows that the relative displacement $(X_2 - X_1)$ gives us an acceleration of m_1 at all frequencies. The condition is that the $Q = \frac{\omega_1 m_1}{B_1}$ has to be high to make the S term small. In the general case, Q of the mechanical spring is very high, in other words $B_1 \sim 0$. Since we have a wide band accelerometer, we can use this wide band acceleration signal as the f_b to cancel the acceleration from m_2. This is just like the method used in appendix B. Therefore it is possible to make a wideband active mass-spring system.

1.2 Motion of an Active Single Mass-Spring System

From Fig.1.1 let us apply feedback by using $f_b = GH(S)(X_1 - X_2)$. The motion equation of the new sytem is

$$m_1 X_1 S^2 + B_1(X_1 - X_2)S + K_1(X_1 - X_2)$$

$$+ GH(S)(X_1 - X_2) = 0 \qquad (1.5)$$

where G is the control gain and H(S) is the frequency compensation function. After solving equation (1.5), we find that

$$X_1 = \frac{\frac{B_1}{m_1}S + \frac{K_1}{m_1}(1 - GH(S))}{S^2 + \frac{B_1}{m_1}S + \frac{K_1}{m_1}(1 - GH(S))} X_2 \qquad . \qquad (1.6)$$

In part 1 I will use $H(S) = 1$, in which case

$$X_1 = \frac{\frac{B_1}{m_1}S + \frac{K_1}{m_1}(1 - G)}{S^2 + \frac{B_1}{m_1}S + \frac{K_1}{m_1}(1 - G)} X_2 \qquad . \qquad (1.7)$$

The new resonant frequency is $\omega_n^2 = \frac{K_1}{m_1}(1 - G)$ where G, which is the over-all gain from sensor to force which is generated by f_b, is close to 1. If $1 - G$ tends toward zero then ω_n tends toward zero too, good noise isolation can be achieved.

Now let us check the stability of the above system by the root-locus method. From appendix C, we know that to make an active double mass-spring system stable is not easy. However, in our new system, the situation looks much

better. The root-locus diagram of equation (1.7) is given by Fig.1.2. It is very clear that this system is always stable. Also, it does not require any special frequency compensation network and the adjustment will be very easy. When the gain of the control system is increased, the Q of this system will be increased because in Fig.1.2, the real part of the pole P is fixed and the imaginary part is reduced from the original. That is why the original Q has to be high, otherwise additional noise will add into this system.

1.3 The Realization of a Prototype Wide Band Superspring System for Ground Motion Isolation

Let us investigate equation (1.7) which is the transfer function of the system in Fig.1.1. The Bode plot of equation (1.7) is shown in Fig.1.3, where $\omega_n^2 = \frac{K_1}{m_1}(1 - G)$. When $1 - G$ and ω_n tend to zero good noise isolation can be achieved in all frequencies which are higher than resonance ω_n. Figure 1.4 shows the relation between the loop gain G and the resonant frequency f^2 which is proportional to the spring constant K.

Now let me explain how the active single mass-spring filter works. From Fig.1.1 the motion of m_2 can go through spring k_1 and B_1 to make m_1 move For example, when m_2 pushes the spring down, then the spring pushes m_1 and m_1 follows m_2 when the frequency of the motion is lower than the resonant frequency. f_b, which is a force generator and controlled by an amplifier which amplifies the signal from
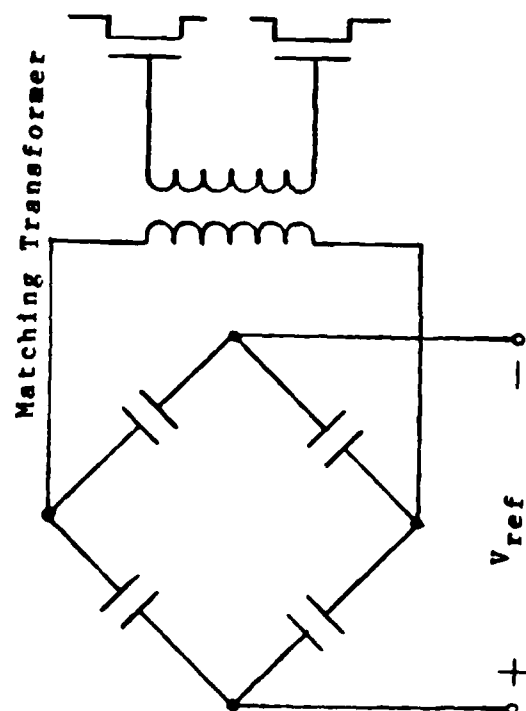
Fig.2.8. The Input Stage of Preamplifier
with a Matching Transformer
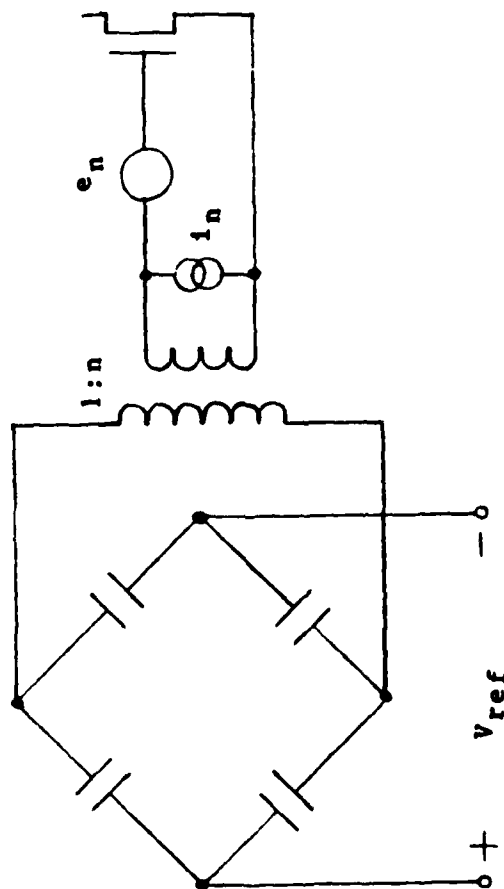
Fig.2.9. The Equivalent Circuit of the Diagram in Fig.3.8

Figure 2.10 gives typical data of an FET's noise performance. We can see clearly that the voltage and current noise are functions of frequency as well as impedance of the capacitor bridge. When the reference frequency increases, the decrease in the impedance of the capacitor is faster than the increase of the current noise. And the voltage noise is decreasing too. After 1--2 MHz, the voltage noise will increase again [Linsay,1982]. Therefore, the signal to noise ratio is better in the high frequency range. However, the gain of the FET will be reduced at high frequencies. This gives, therefore, a kind of trade off between the gain and signal to noise ratio.

The whole circuit of the preamplifier stages is described in Fig.2.11. The operating point of the first differential FET amplifier is chosen at 10mA in order to reduce the voltage noise. The tank circuit works at 200KHz in order to reduce the second harmonic distortion. By using a transformer, the D.C. component in the capacitor bridge can be balanced by adjusting a potentiometer which is connected on the primary coil. The other advantage is that the common mode rejection of a transformer is a constant. It is not like the common mode rejection of a differential amplifier which is a function of the common mode voltage.

b.   Demodulator

The signal from the bridge is shown is Fig.2.3. It has the phase and amplitude information which is modulated by
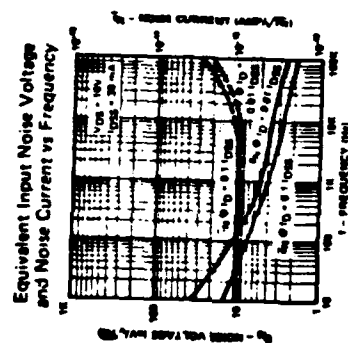
Fig.2.10. Noise Performance of 2N5564 FET[Siliconix Inc.]

the motion of the mass. In order to recover the modulating signal, a synchronized detector is required. Due to the $\frac{1}{f}$ noise, white noise and the limited frequency range, a multiplier circuit is not desired. Therefore, an analog switch circuit plus phase shift circuit has been conceived to demodulate the signal shown in Fig.2.3. The circuit is shown in Fig.2.12. The noise from the switch circuit is mainly due to the timing of the two out of phase trigger square waves. These two trigger signals have to be 180° out of phase. If these two trigger's do not have a 180° phase difference, it will cause a noisy output. That is why I use two digital gates to make the trigger have correct timing from the single square wave output. In order to make the analog switch work under high frequency conditions, a load resistor is required, otherwise, the charge or the current in the switch has no way to dissipate during the switching time. The phase shift circuit is shown in Fig.2.13. When the potentiometer equals zero, this operational amplifier operates like a voltage follower with zero phase shift. When the potentiometer equals 200KΩ , which is taken as an open circuit, the operational amplifier operates like an inverter with 180° phase shift. The transfer function is given by

$$\frac{V_{out}}{V_{in}} = \frac{R_1 - Z}{R_1 + Z} \text{ or } \left|\frac{V_{out}}{V_{in}}\right| = 1 \;,\; \theta = tg^{-1} = \frac{2 \times R_1 \times \omega c}{1 - (R \times_1 \omega c)^2}$$

$$(2.21)$$

where $Z = \frac{1}{j\omega c}$. When $R_1 = 0$, $\frac{V_{out}}{V_{in}} = 1$, there is no phase
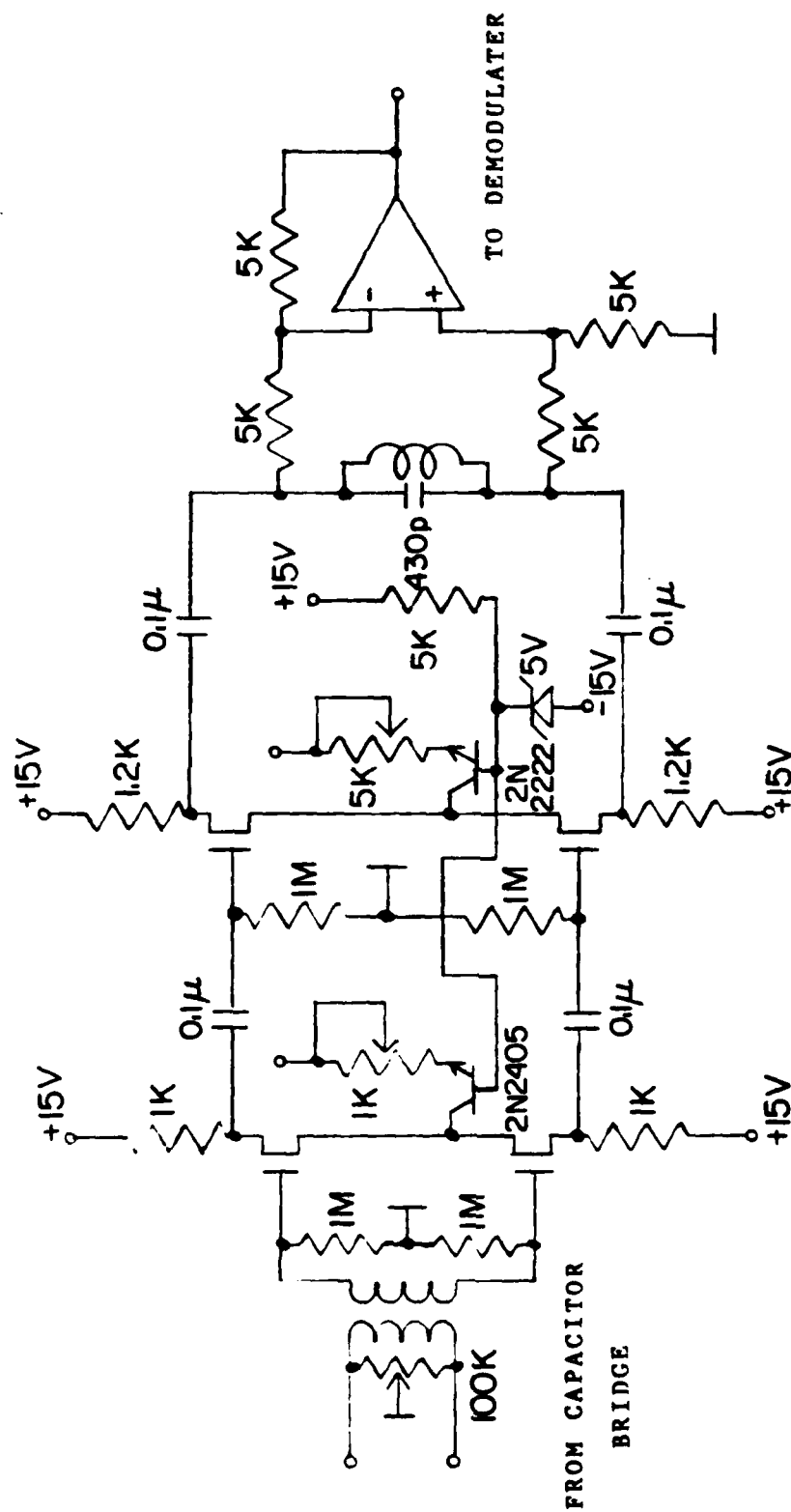
Fig.2.11. The Circuit Diagram of the Preamplifies Stages

Fig.2.2.12. The Circuitry of the Demodulator
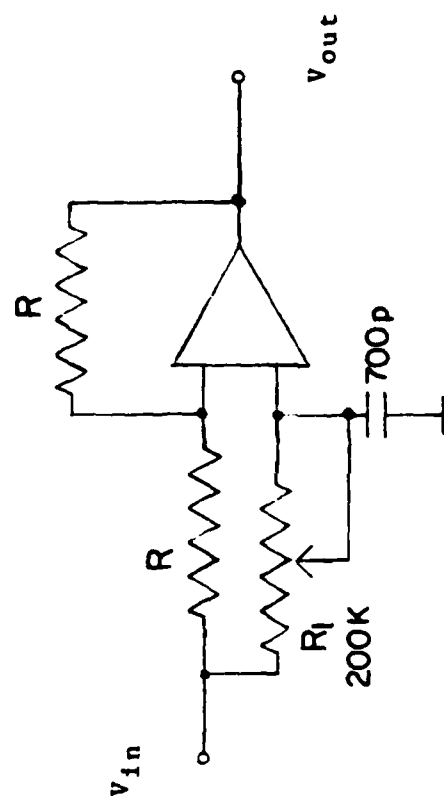
Fig.2.13. The Diagram of the Phase Shift Circuit

shift. When $R_1 \gg Z$, $\dfrac{V_{out}}{V_{in}} = -1$, there is phase shift by 180°. When $0 < R_1 < 200$ KΩ , there is phase shift between $0°$ to $180°$ depends on value of R_1.

c. V - I Converter

In this portion of the circuit, a coil which is moving in a magnetic field to produce a force has been used. Because the force, produced by the coil, is proportional to current going through the coil, a voltage to current converter is required.

In our system, the total mass is about 20Kg. In order to move this kind of big mass, a big force has to be applied to this mass. Also, a big current through the coil is necessary. Therefore, a V - I converter has to be made by using some large power transistor. In general, the large power transistor is very noisy. In these experiments, a feedback circuit is applied with a large amount of feedback, the circuit being shown in Fig.2.14. The V - I gain equals one, so the noise in the output can be neglected.

d. Compensation Filter

In the appendix B, I discuss that the characteristics of an active mass-spring system depend on what kind of features of the feedback network is required. For example, for the velocity term, a differentiation network is required. Since a differentiation circuit is very noisy at high frequencies, we need a low-pass filter to work with the differentiation filter. In other words, it is a bandpass filter which gives the differential function in some
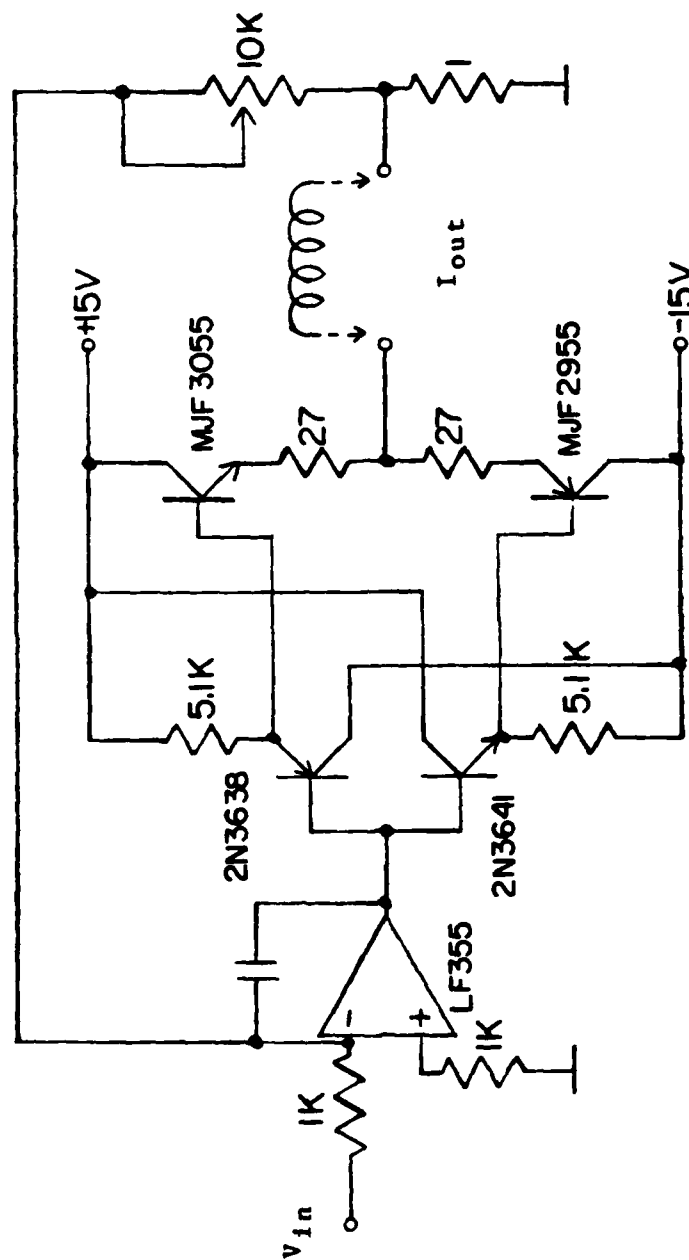
Fig.2.14. A Diagram of the V – I Converter

frequency range. Also, having the resonant frequency of the filter variable is very useful. The compensation filter is shown in Fig.2.15 [Ghausi], with the detailed analysis following. Let us redraw the bandpass filter part of the compensation filter in Fig.2.16. The transfer function is given by [Ghausi]

$$\frac{V_2}{V_{in}} = \frac{\dfrac{G_1 G_2}{1 - \dfrac{1}{K}}}{S^2 + S(G_2 S_1 + G_1 S_2 - \dfrac{G_1 G_2}{K-1}) + G_1 G_2 S_1 S_2} \qquad (2.22)$$

where $G_i = \dfrac{1}{R_i}$; $S_1 = \dfrac{1}{C_i}$ and $K = 1 + \dfrac{R_a}{R_b}$. Let $C_1 = C_2 = 1 \ \mu F$; $R_2 = 10 \ R_1$; $R_b = 1 \ K\Omega$ and $f_0 = 100 \ Hz$. We can find that $R_1 = 0.5 \ K\Omega$ and $R_2 = 5 \ K\Omega$. Let R_1 and R_2 change at the same time. We get a variable resonant frequency bandpass filter. Therefore, the transfer function is

$$\frac{V_2}{V_{IN}} = \frac{- 4 \times 10^{-7} S}{S^2 + 400S + 628^2} \qquad . \qquad (2.23)$$

Let us look at the integration part in Fig.2.15. The transfer function is given by

$$H(S) = \frac{1}{RCS} \qquad . \qquad (2.24)$$

by setting $R = 50 \ K\Omega$, $C = 1 \ \mu F$; we get

$$H(S) = \frac{1}{50S} \qquad . \qquad (2.25)$$
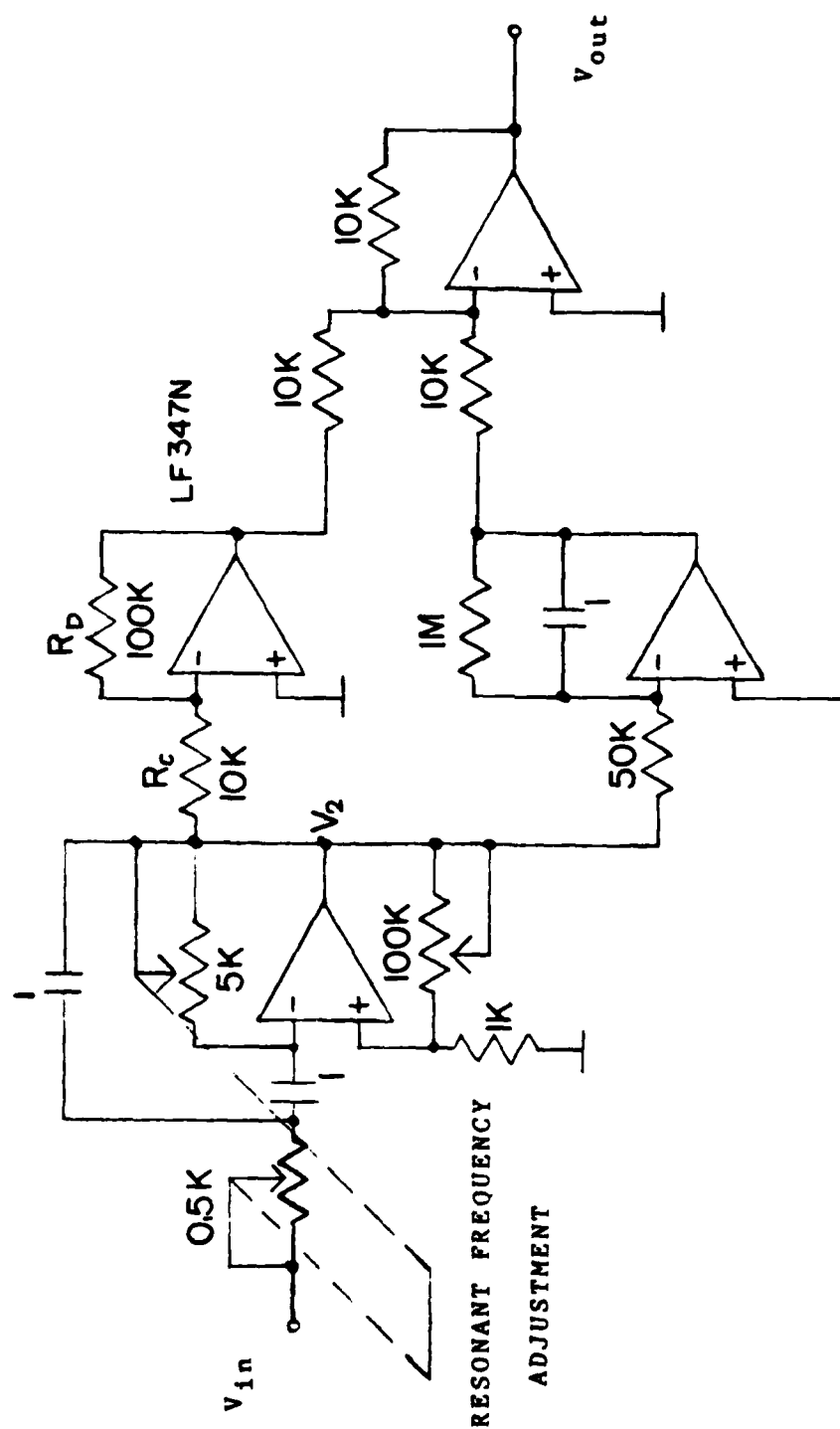
Fig.2.15. The Circuit Diagram of the Frequency Compensation Filter
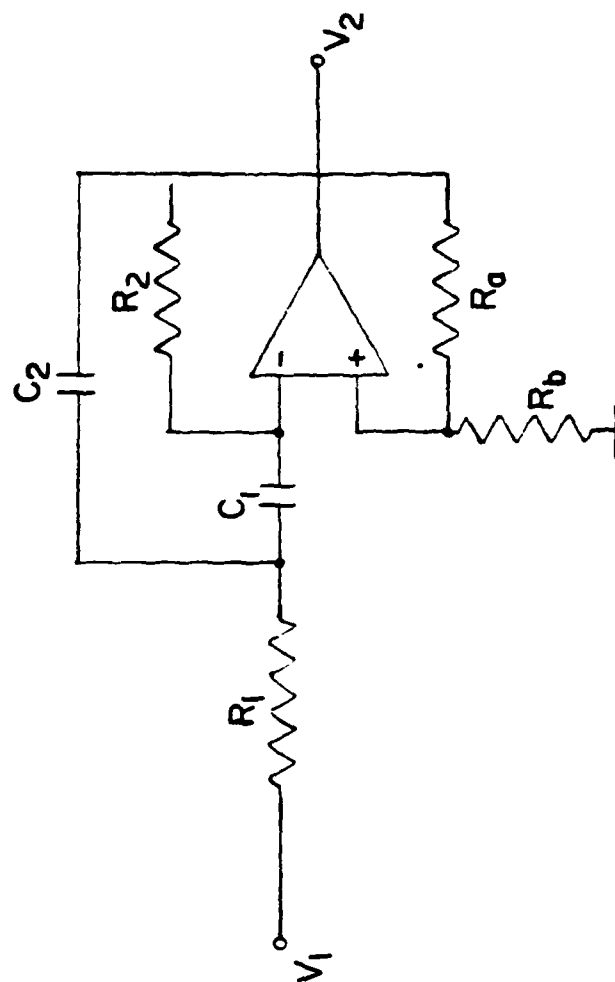
Fig.2.16. A Portion of Fig.2.15

Now, let us go back to Fig.2.15. The overall transfer function is given by

$$\frac{V_{out}}{V_{in}} = \frac{K \times 4 \times 10^{-7} + 20 \times 4 \times 10^{-7}}{S^2 + 400S + 628^2} \quad . \quad (2.26)$$

The advantage of this filter is that we can get different transfer functions between different nodes. It is very convenient for being able to make different frequency compensations.

The design of the electrical control circuit is completed. The $\frac{1}{f}$ noise due to the amplifiers is limited. The white noise is dominated by the voltage noise of the FET in the preamplifier. The sensitivty is high enough to pick up the weak ground motion. The next chapter will discuss the mechanical structure of the wideband superspring.

CHAPTER 3

MECHANICAL DESIGN

In this chapter discussion is given on the structure of the active single mass-spring low-pass filter from the sensor to the force converter, a so-called wide band superspring. And mainly, a study is made of how to confirm the motion of the mass in one direction.

3.1. Construction of the Sensor

From the last chapter, we know that the signal from the four variable capacitors bridge is four times bigger than from the one variable capacitor bridge. The design of the capacitor bridge is dependent on four variables. The structure is shown in Fig.3.1. The middle fibre glass rod is connected to the mass and spring combination. When the mass is moving, the capacitances between the plates are changing. The capacitance between two plates is about 300pF. All the plates are made of aluminum and lapped to 2.5×10^{-5} m flatness.

3.2. Current-Force Converter

The structure of the converter is shown in Fig.3.2. In order to get a big magnetic field in the small gap $(62.5 \times 10^{-5}$ m), μ — metal is used to guide the magnetic field to the gap. The two flexures are used to confirm the coil to move up and down only without contacting μ — metal. The centre rod is used to connect the displacement sensor and mass. The equation of the force vs current is given by [Chen,1983]
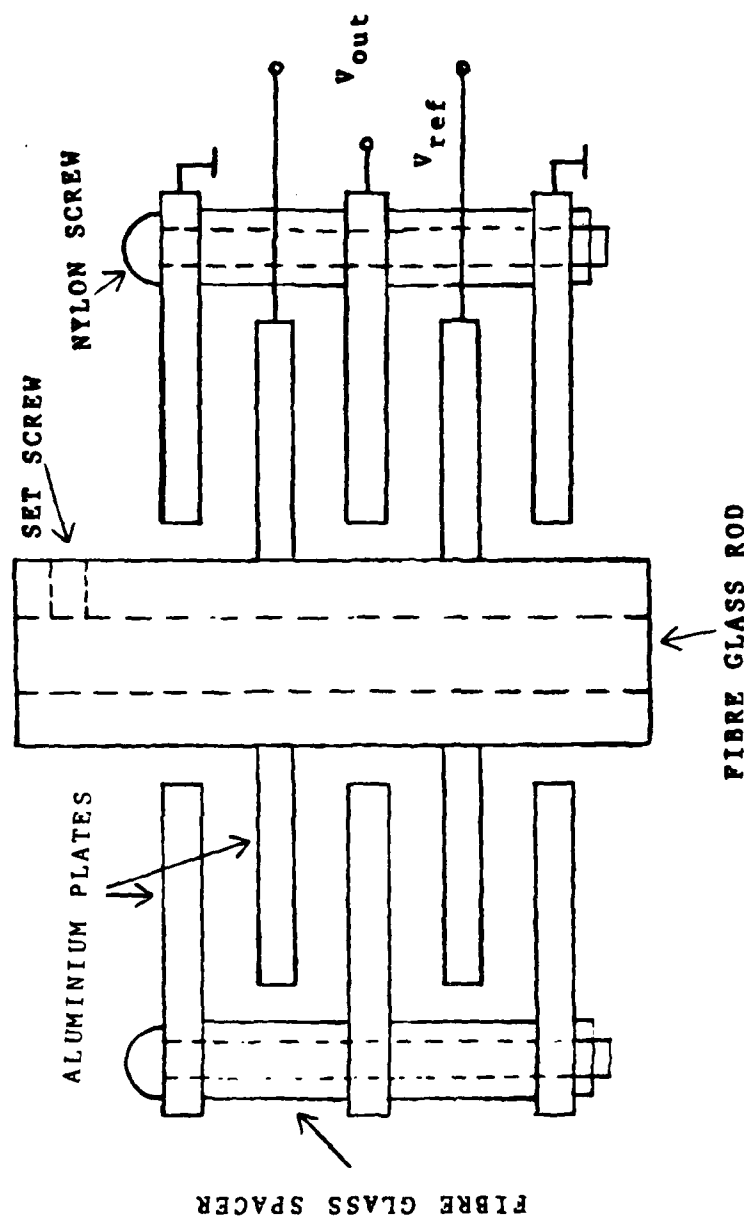
Fig.3.1. The Structure of the Four Variable Capacitor Bridge

$$f = 0.1B\pi DNI \quad \text{dynes} \tag{3.1}$$

where B (in gauss) is the radial flux density in the air gap, D (in cm) is the mean diameter of the coil, N is the number of the turns of the coil and I (in amp.) represents the control current. In equation (3.1), the force f is linearly proportional to the current I. Therefore, this converter looks like the force generator f_b.

3.3. Control of Spring Modes

In a mass-spring system the spring has at least five different modes of oscillation. As shown in Fig.3.3, all these different modes have different phase and amplitude relationships with the main mode. When the main mode is fedback in phase, the other modes are out of phase. That is likely to cause oscillations. These oscillations will saturate the preamplifier as well as make the mass have a large oscillatory motion causing the system to be non-adjustable. In my system there are three pieces of flexure to confirm the main spring and mass. A simple schematic is shown in Fig.3.4. These flexures control the wobble, pendulum, and torsion modes while the plastic foam gives a big damping factor to violin string and accordian modes. The flexure is shown in Fig.3.5. In order to reduce the can factor from the flexure, this flexure only has two circle springs, it is thus not like others which have three or four circle springs [Rinker III,1983], and three gaps at the

outside circle.

The whole test set is shown in the next chapter (Fig.4.1). The mass in Fig.4.1 is well defined for one directional motion only. It makes the control loop easy to adjust, otherwise the additional modes of these springs will cause failure of test.
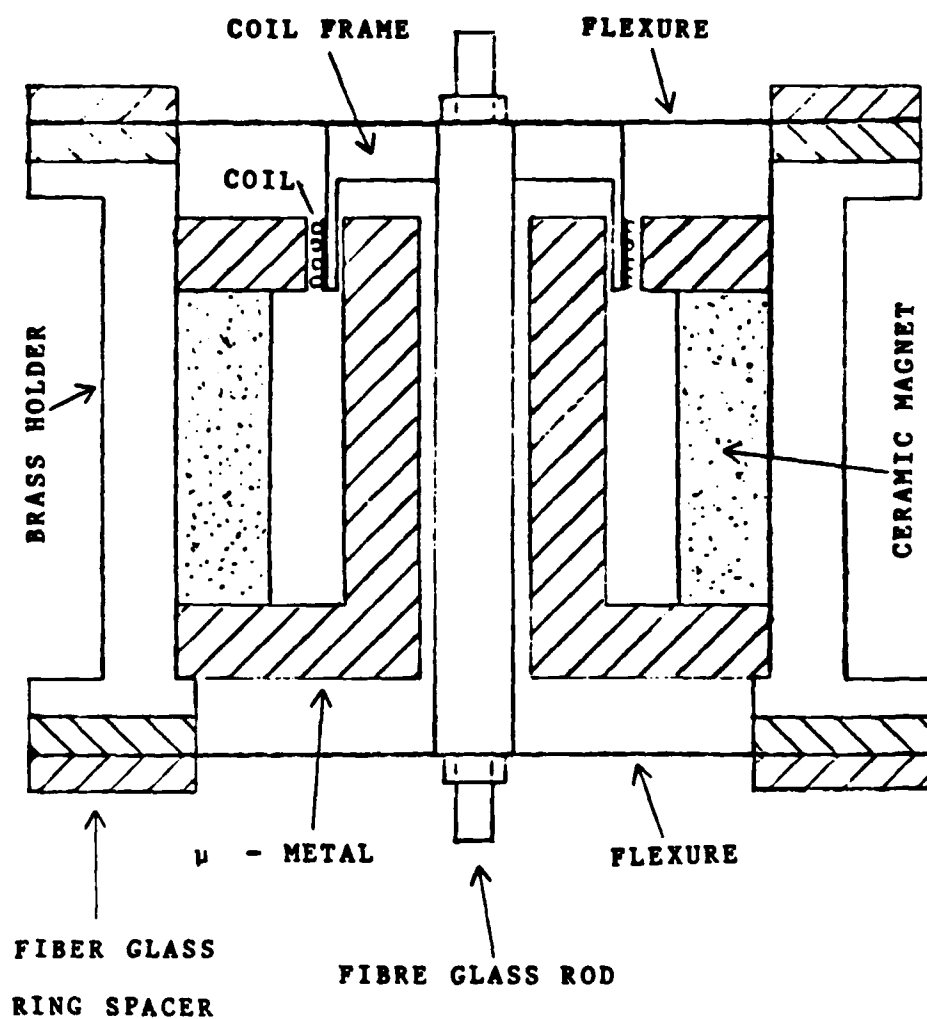
Fig.3.2. The Cross Structure of the Force Converter

WOBBLE
MODE

PENDULUM
MODE

TORSION
MODE

VIOLIN STRING
MODE

ACCORDIAN
MODE
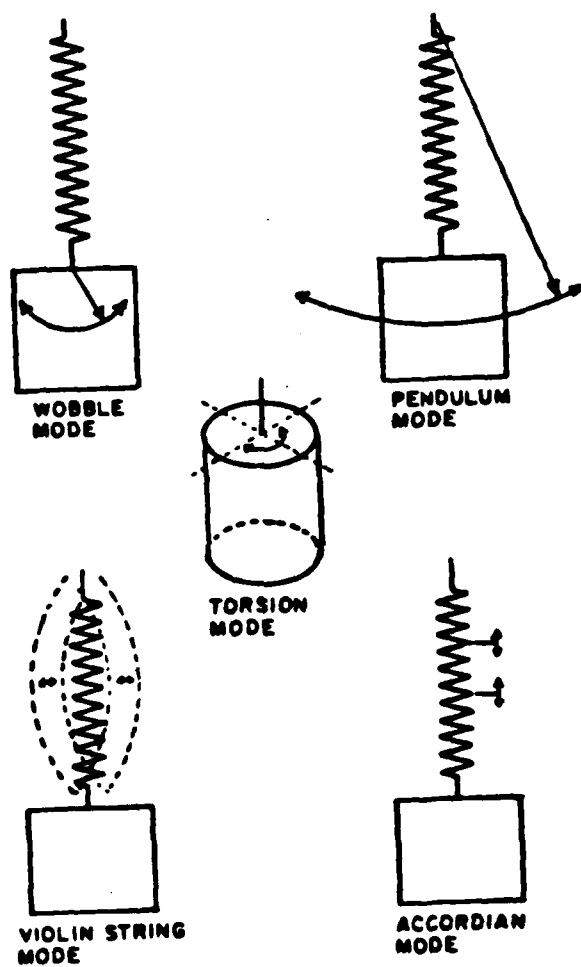
Fig.3.3. The Modes of Osillation of a Mass-Spring System

Fig.3.4. The Control of the Different Modes
in the Main Spring

GAP

CIRCLE SPRING

Fig.3.5. Top View of the Flexure

CHAPTER 4

PERFORMANCE OF THE ACTIVE SINGLE MASS-SPRING
LOW-PASS FILTER FOR GROUND MOTION ISOLATION

Since we studied all parts of a wideband superspring,we are ready to test it. In this chapter, a test result of the superspring will be discussed.

In oeder to test the low-pass filter charactristic of the superspring, we need an accelerometer to measure the acceleration of the platform (mass). I used an accelerometer, which was developed by Dr. Moody in our Lab, and was attached to the platform. The housing of this accelerometer is the mass itself which is shown in Fig.4.1. The output of the accelerometer is the acceleration at the mass due to the force from the springs.

The whole set of the active mass-spring system is shown in Fig.4.1. The middle accelerometer, which can tell us how much the acceleration has dropped after the feedback loop is closed and the gain of the loop is varied, is used for independent checking. Also the weight of the accelerometer is a part of the platform. The block diagram of the electrical circuit is shown in Fig.2.1. The electrical circuit represents the methmatical function $f_b = GH(S)(X_1 - X_2)$, as shown in section 1.2. Equation (1.7) discribes the motion of the active filter. The output signal of the accelerometer (Fig.4.3.) shows that the resonant frequency of the superspring is shifted down when the feedback loop is closed.

Fig.4.1. The Structure of the Active Single
Mass-Spring System

Table 1. shows the resulting data where f^2 is proportional to the spring constant k_1 in Fig 1.1. When the gain of the loop is increasing, the resonant frequency and the spring constant are decreasing. Figure 4.2 shows that the relationship of frequency vs spring constant is a straight line. Figure 4.3 gives a very clear view of the ground motion isolation characteristic of the active mass-spring system. Figure 4.3a shows the acceleration on the mass with the control loop open. Then Fig.4.3b,c,d show that the resonant frequency of the superspring is shifted down to 2.2 Hz, 2.0 Hz and 1.2 Hz, correspondingly. It is seen that the acceleration of mass is slowed down, when comparied with the upper trace, which is open loop acceleration of the mass.

Now, let us compare the experimental results, as shown in Fig.4.2 with the theoretical value which was developed in chapter 1 and as shown in Fig.1.4. They are both a straight line with negative slope and almost identical except below 1 Hz. This is very strong proof that the wideband superspring is a very good ground motion isolation system not only in theory but also in practice.

$f^2(Hz)^2$	$f(Hz)$	G
4	2	4.86×10^{-3}
9	3	4.35×10^{-3}
11.56	3.4	3.87×10^{-3}
14.44	3.8	3.44×10^{-3}
17.64	4.2	3.07×10^{-3}
21.16	4.6	2.72×10^{-3}
23.04	4.8	2.17×10^{-3}
29.16	5.4	1.70×10^{-3}
31.36	5.6	1.17×10^{-3}
34.81	5.9	7.63×10^{-4}
36	6	4.16×10^{-4}
39.69	6.3	6.52×10^{-5}
40.96	6.4	0

Table 1. The Data of the Result
where G is measured from the output of the modulator
to the output of the V - I converter

Fig.4.2. The Picture of the Data

Fig.4.3. The Output of Acceleration of the Mass Where the Upper Trace is not Controlled and the Lower Trace is After Control is applied

PART II

A MASS-SPRING SYSTEM AT LOW TEMPERATURES

CHAPTER 5

SUPERCONDUCTING MASS-SPRING SYSTEM

The previous chapters discussed passive and active mass-spring systems. Due to thermal noise, the sensitivity of an accelerometer is limited to $10^{-9} gHz^{-1/2}$. In order to increase the sensitivity and decrease the thermal noise, we have to use low temperature devices because the thermal noise is proportional to the temperature.

This chapter will discuss a superconducting accelerometer which uses a SQUID amplifier which has sensitivity approaching $0.1 \times 10^{-18} Wb$ ($10^{-11} gauss \ cm^2$). The sensitivity of the superconducting accelerometer is about 10^{-13}[Chan,1982]. Due to its contribution to high sensitivity, the Q of the accelerometer is a very serious problem. It can cause the SQUID to unlock. The Q of a Nb superconducting accelerometer is about 50×10^3 under a pressure equal to 4×10^{-5} TORR. A high output voltage at the resonance frequency will saturate the SQUID amplifier which puts a limit on the sensitivity. In order to make the sensitivity high, the Q of the superconducting accelerometer has to be controlled. This chapter will describe two different methods to reduce the Q of the superconducting accelerometer without decreasing the sensitivity in the signal range.

5.1. Superconducting Displacement Sensor[Paik,1974]

Superconducting materials form almost perfect

electromagnatic shields. The total magnetic flux threading a superconducting loop cannot change as long as the circuit remains resistanceless. This flux is

$$\phi = LI = constant \qquad .$$

(5.1)

If the inductance L is increased, the persistent current, I, will decrease to keep the magnetic flux ϕ constant. That is

$$L_1 I_1 = L_1' I_1' = \phi$$

(5.2)

where L_1' and I_1' are the values after changing L_1 and I_1. This is the fundamental principle of a superconducting displacement sensor. A schematic of a superconducting displacement sensor is shown in Fig.5.1. In Fig.5.1 the inductance L_1 is a function of d[Paik,1974]. When d is changed by movement of the mass, the value of L_1 is modulated by d. Since the flux ϕ is a constant, the current I_1 has to be changed too. This can be represented as

$$\nabla I = I_1 - I_1' = I_1 \left(\frac{L_1' - L_1}{L_1} \right) = I_1 \left(1 - \frac{L_1}{L_1'} \right) \qquad .$$

(5.3)

Then ∇I will be coupled to the SQUID by the inductor L_2. Therefore, the output of the SQUID is proportional to the displacement d between L_1 and the mass shown in Fig.5.1.

Fig.5.1. A Schematic of a Superconducting Displacemnet Sensor

When the persistent I_1 and L_1' are bigger then VI will be higher, from equation (5.3). In other words, using a big persistent current and small gap between the mass and coil, the sensitivity of the displacement sensor will be high. That is why we always try to store a big current in a superconducting accelerometer. However, due to the high Q (50×10^3), we cannot store too large a current, otherwise, the peak of the resonant frequency will saturate the SQUID amplifier. In order to increase the sensitivity of a superconducting accelerometer, we have to reduce its Q. The next two sections will discuss two different ways to reduce Q.

5.2. Reduction of Q by Electromechanical Feedback Control

A simple experimental setup is shown in Fig.5.2. The gravity gradiometer consists of two superconducting accelerometers which are worked in a differential mode. This structure is equivalent to the double mass-spring system shown in Fig.A.1, where the m_1, k_1 and B_1 are associated with the accelerometer in the gradiometer. Therefore, we can set $GH(S) = \frac{G}{S}$ in equation (B.9). Then we get

$$X_1 = \frac{(\frac{B_2}{m_2}S + \frac{K_2}{m_2})(\frac{B_1}{m_1}S + \frac{K_1}{m_1})X_3}{(S^2 + \frac{B_2}{m_2} + \frac{K_2}{m_2})(S^2 + (\frac{B_1}{m_1} + \frac{G}{m_2})S + \frac{K_1}{m_1})} \quad . \quad (5.4)$$

The Q of the accelerometer is given by

FIG.5.2. The Experimental Setup

$$Q = \cfrac{\omega_0}{\cfrac{B_1}{m_1} + \cfrac{G}{m_2}}$$
(5.5)

where $\omega_0^2 = (\frac{K_1}{m_1})$. When the control gain G is increased, Q is reduced. Dependent on this concept, a control circuit is shown in Fig.5.2. The bandpass filter is made by cascading a high pass and a low-pass filter. This bandpass filter makes the gain higher at the resonant frequency and the gain lower elsewhere. This filter will limit the noise of the control circuit in the signal range. Figure 5.3 shows test results. The resonant frequency of 19.8 Hz was dropped about 20 db. From equation (5.5), Q can be reduced to 1. But here it is lowered about 20db. The reason is that the gradiometer consists of two accelerometers. They have resonant frequencies which differ only a little and they are out of phase with each other. Therefore, after 19.8 Hz is lowered the other resonance peak will be driven if the gain and phase are right. But the electromechanical damping cannot give us more attenuation in this special structure. We need to find some other way. The next section will discuss a electronic damping method.

5.3. Electronic Damping [Wang,1979]

A mass-spring accelerometer, as shown in Fig.5.1 can be represented by an LCR circuit as shown in Fig.5.4. If we have some ways to increase the resistance R, the Q of the LC circuit will be reduced. A simple block diagram is shown in Fig.5.5. An additional electronic resistor is introduced by

Fig.5.3. The Test Result of the Mechanical Cool Damping

a. The Output of the Gradiometer with the Feedback Loop Open

b. The Output of the Gradiometer with the Feedback Loop Closed

Fig.5.4.The equivalent circuit of Fig.5.1

69

FIG.5.5. A Cool Damping Block Diagram for an Equivalent RLC

Accelerameter[Wang,1979]

$\dfrac{V_f(S)}{I(S)}$ in the signal pickup loop. The new Q factor is

$R + \dfrac{V_f(S)}{I(S)}$. If we can control $\dfrac{V_f(S)}{I(S)}$, we can control the Q of the LCR circuit. In Fig.5.5 the electronic resistance is given by

$$\frac{V_f(S)}{V_s(S)} = GH(S) = R_e \qquad . \qquad\qquad (5.6)$$

Because we are only interested in the behavior at the resonance, $H(S)$ can be a bandpass filter, as $H(S) \dfrac{CS}{S^2 + AS + B}$ which has a high gain at the resonance frequency. When the gain G, in equation (5.6), is increased, the resistance R is increased and the Q of the RLC circuit is decreased. The actual block digram is shown in Fig.2.15 from V_{in} to V_1. This bandpass filter has a 50db difference in the frequency range from 0.5 Hz to 20 Hz. The test results are shown in Fig.5.7. The resonant frequency 19.6 Hz is dropped about 40db.

5.4.Minimum Q Achievable [Wang,1979;Mapoles,1980]

From equation (5.6), R_e may be as large as we want by increasing the gain of the feedback path. Thus it would seem that the Q of the accelerometer can be made as low as desired. This is not quite possible in practice, since the current induced by $V_f(S)$ in the input of the SQUID in Fig.5.5 is not considered in this model. Actually the current detected by the SQUID is the difference of the

Fig.5.6. A Block Diagram of Electronic Cool Damp for an Accelerometer
where M is the Mutual Inductance between L and L_2

Fig.3.4. The Control of the Different Modes
in the Main Spring

GAP

CIRCLE SPRING

Fig.3.5. Top View of the Flexure

CHAPTER 4

PERFORMANCE OF THE ACTIVE SINGLE MASS-SPRING

LOW-PASS FILTER FOR GROUND MOTION ISOLATION

Since we studied all parts of a wideband superspring, we are ready to test it. In this chapter, a test result of the superspring will be discussed.

In oeder to test the low-pass filter charactristic of the superspring, we need an accelerometer to measure the acceleration of the platform (mass). I used an accelerometer, which was developed by Dr. Moody in our Lab, and was attached to the platform. The housing of this accelerometer is the mass itself which is shown in Fig.4.1. The output of the accelerometer is the acceleration at the mass due to the force from the springs.

The whole set of the active mass-spring system is shown in Fig.4.1. The middle accelerometer, which can tell us how much the acceleration has dropped after the feedback loop is closed and the gain of the loop is varied, is used for independent checking. Also the weight of the accelerometer is a part of the platform. The block diagram of the electrical circuit is shown in Fig.2.1. The electrical circuit represents the methmatical function $f_b = GH(S)(X_1 - X_2)$, as shown in section 1.2. Equation (1.7) discribes the motion of the active filter. The output signal of the accelerometer (Fig.4.3.) shows that the resonant frequency of the superspring is shifted down when the feedback loop is closed.

Fig.4.1. The Structure of the Active Single

Mass-Spring System

Table 1. shows the resulting data where f^2 is proportional to the spring constant k_1 in Fig 1.1. When the gain of the loop is increasing, the resonant frequency and the spring constant are decreasing. Figure 4.2 shows that the relationship of frequency vs spring constant is a straight line. Figure 4.3 gives a very clear view of the ground motion isolation characteristic of the active mass-spring system. Figure 4.3a shows the acceleration on the mass with the control loop open. Then Fig.4.3b,c,d show that the resonant frequency of the superspring is shifted down to 2.2 Hz, 2.0 Hz and 1.2 Hz, correspondingly. It is seen that the acceleration of mass is slowed down, when comparied with the upper trace, which is open loop acceleration of the mass.

Now, let us compare the experimental results, as shown in Fig.4.2 with the theoretical value which was developed in chapter 1 and as shown in Fig.1.4. They are both a straight line with negative slope and almost identical except below 1 Hz. This is very strong proof that the wideband superspring is a very good ground motion isolation system not only in theory but also in practice.

$f^2(Hz)^2$	$f(Hz)$	G
4	2	4.86×10^{-3}
9	3	4.35×10^{-3}
11.56	3.4	3.87×10^{-3}
14.44	3.8	3.44×10^{-3}
17.64	4.2	3.07×10^{-3}
21.16	4.6	2.72×10^{-3}
23.04	4.8	2.17×10^{-3}
29.16	5.4	1.70×10^{-3}
31.36	5.6	1.17×10^{-3}
34.81	5.9	7.63×10^{-4}
36	6	4.16×10^{-4}
39.69	6.3	6.52×10^{-5}
40.96	6.4	0

Table 1. The Data of the Result
where G is measured from the output of the modulator
to the output of the V - I converter

Fig.4.2. The Picture of the Data

59

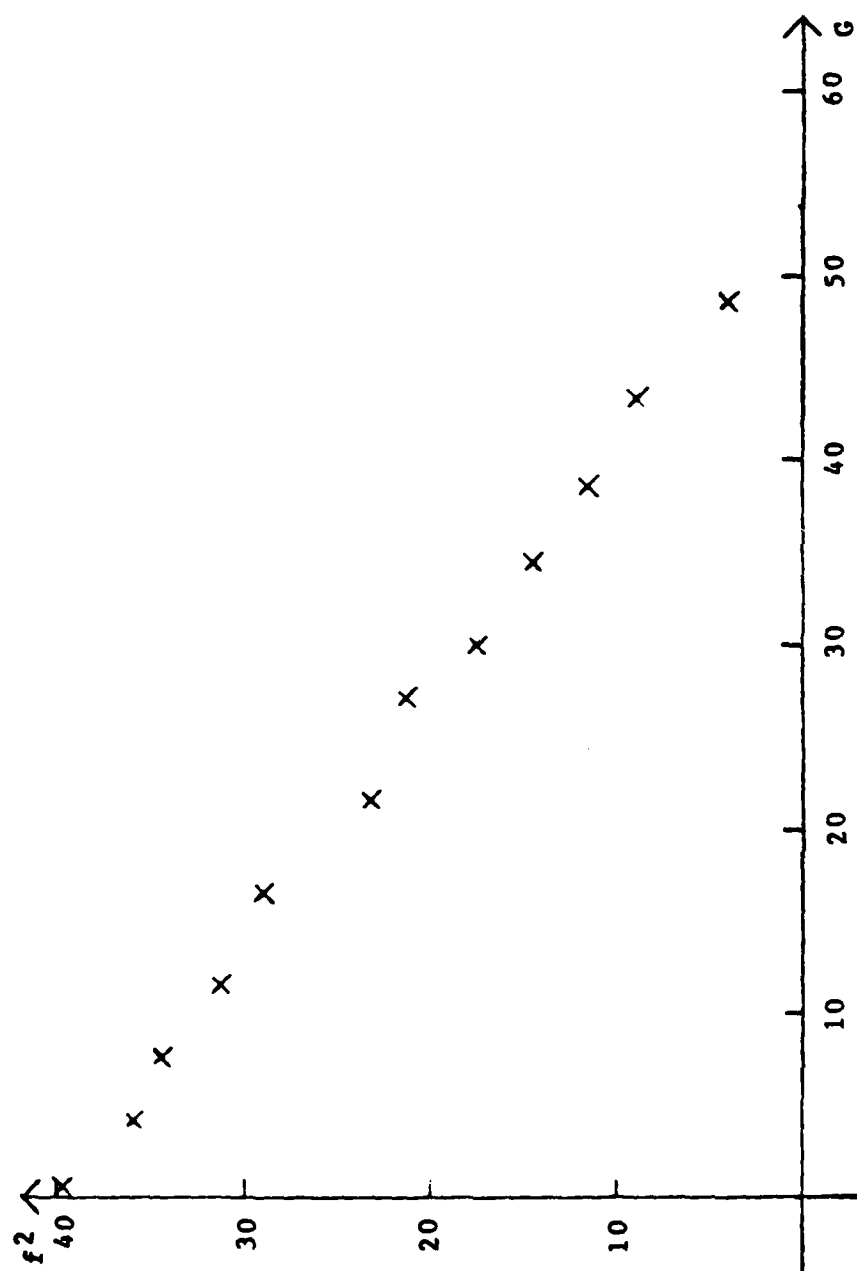Fig.4.3. The Output of Acceleration of the Mass Where the Upper Trace is not Controlled and the Lower Trace is After Control is applied

PART II

A MASS-SPRING SYSTEM AT LOW TEMPERATURES

CHAPTER 5

SUPERCONDUCTING MASS-SPRING SYSTEM

The previous chapters discussed passive and active mass-spring systems. Due to thermal noise, the sensitivity of an accelerometer is limited to $10^{-9} gHz^{-1/2}$. In order to increase the sensitivity and decrease the thermal noise, we have to use low temperature devices because the thermal noise is proportional to the temperature.

This chapter will discuss a superconducting accelerometer which uses a SQUID amplifier which has sensitivity approaching $0.1x10^{-18}Wb$ ($10^{-11}gauss$ cm^2). The sensitivity of the superconducting accelerometer is about 10^{-13}[Chan,1982]. Due to its contribution to high sensitivity, the Q of the accelerometer is a very serious problem. It can cause the SQUID to unlock. The Q of a Nb superconducting accelerometer is about $50x10^3$ under a pressure equal to $4x10^{-5}$ TORR. A high output voltage at the resonance frequency will saturate the SQUID amplifier which puts a limit on the sensitivity. In order to make the sensitivity high, the Q of the superconducting accelerometer has to be controlled. This chapter will describe two different methods to reduce the Q of the superconducting accelerometer without decreasing the sensitivity in the signal range.

5.1. Superconducting Displacement Sensor[Paik,1974]

Superconducting materials form almost perfect

electromagnatic shields. The total magnetic flux threading a superconducting loop cannot change as long as the circuit remains resistanceless. This flux is

$$\phi = LI = \text{constant} \quad . \tag{5.1}$$

If the inductance L is increased, the persistent current, I, will decrease to keep the magnetic flux ϕ constant. That is

$$L_1 I_1 = L_1' I_1' = \phi \tag{5.2}$$

where L_1' and I_1' are the values after changing L_1 and I_1. This is the fundamental principle of a superconducting displacement sensor. A schematic of a superconducting displacement sensor is shown in Fig.5.1. In Fig.5.1 the inductance L_1 is a function of d[Paik,1974]. When d is changed by movement of the mass, the value of L_1 is modulated by d. Since the flux ϕ is a constant, the current I_1 has to be changed too. This can be represented as

$$\nabla I = I_1 - I_1' = I_1 \left(\frac{L_1' - L_1}{L_1} \right) = I_1 \left(1 - \frac{L_1}{L_1'} \right) \quad . \tag{5.3}$$

Then ∇I will be coupled to the SQUID by the inductor L_2. Therefore, the output of the SQUID is proportional to the displacement d between L_1 and the mass shown in Fig.5.1.

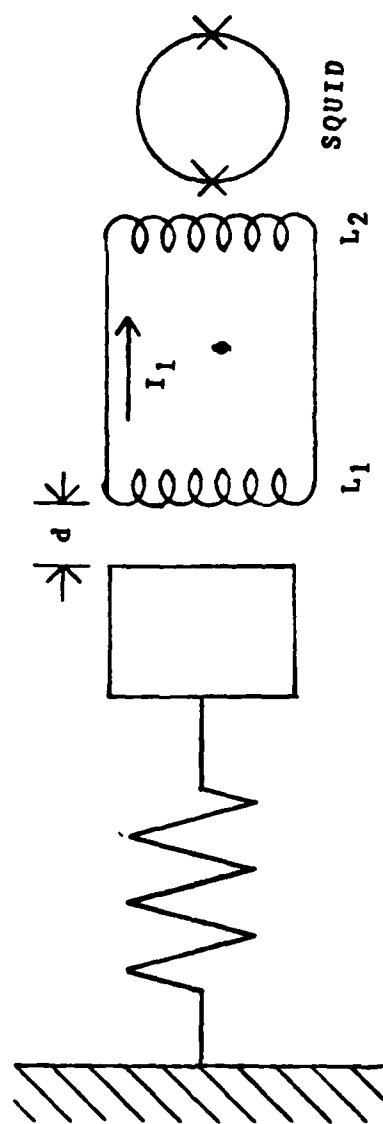NIOBIUM MASS   SUPERCONDUCTING COILS

L_1

L_2

I_1

d

SQUID

Fig.5.1. A Schematic of a Superconducting Displacemnet Sensor

When the persistent I_1 and L_1' are bigger then ∇I will be higher, from equation (5.3). In other words, using a big persistent current and small gap between the mass and coil, the sensitivity of the displacement sensor will be high. That is why we always try to store a big current in a superconducting accelerometer. However, due to the high Q (50×10^3), we cannot store too large a current, otherwise, the peak of the resonant frequency will saturate the SQUID amplifier. In order to increase the sensitivity of a superconducting accelerometer, we have to reduce its Q. The next two sections will discuss two different ways to reduce Q.

5.2. Reduction of Q by Electromechanical Feedback Control

A simple experimental setup is shown in Fig.5.2. The gravity gradiometer consists of two superconducting accelerometers which are worked in a differential mode. This structure is equivalent to the double mass-spring system shown in Fig.A.1, where the m_1, k_1 and B_1 are associated with the accelerometer in the gradiometer. Therefore, we can set $GH(S) = \dfrac{G}{S}$ in equation (B.9). Then we get

$$X_1 = \frac{(\frac{B_2}{m_2}S + \frac{K_2}{m_2})(\frac{B_1}{m_1}S + \frac{K_1}{m_1})X_3}{(S^2 + \frac{B_2}{m_2} + \frac{K_2}{m_2})(S^2 + (\frac{B_1}{m_1} + \frac{G}{m_2})S + \frac{K_1}{m_1})} \qquad (5.4)$$

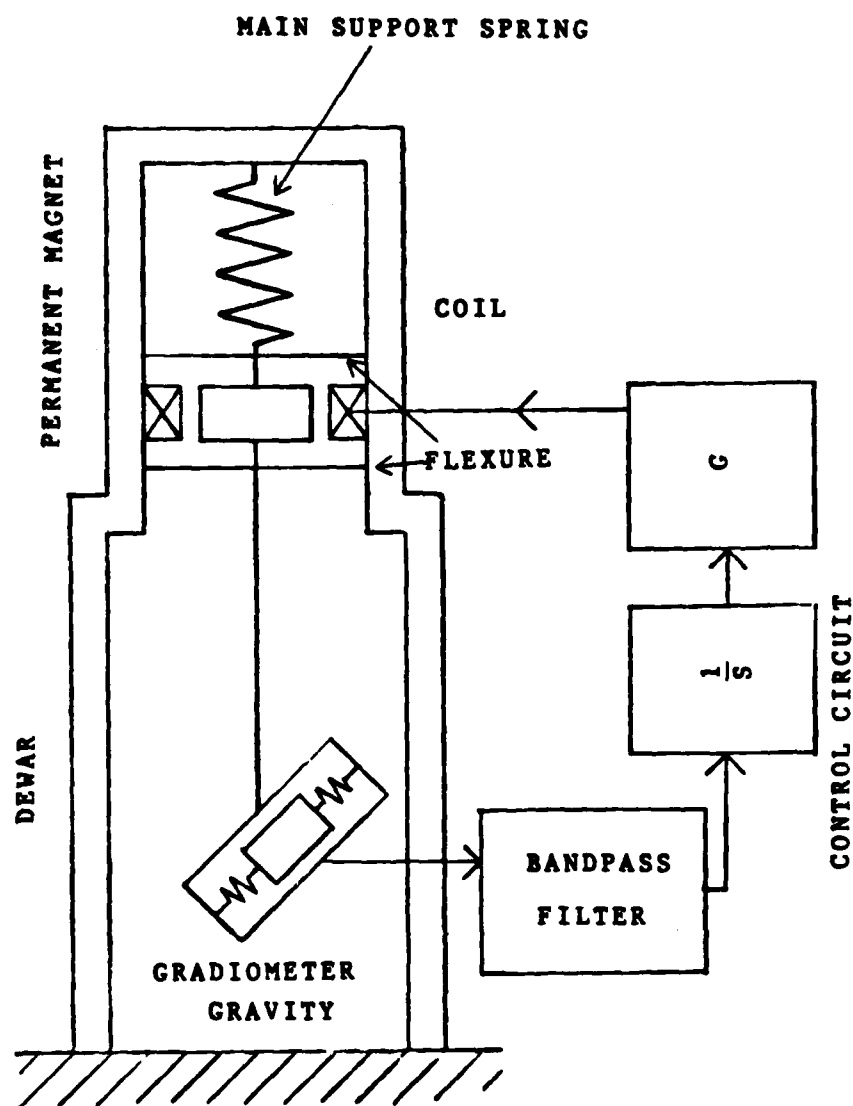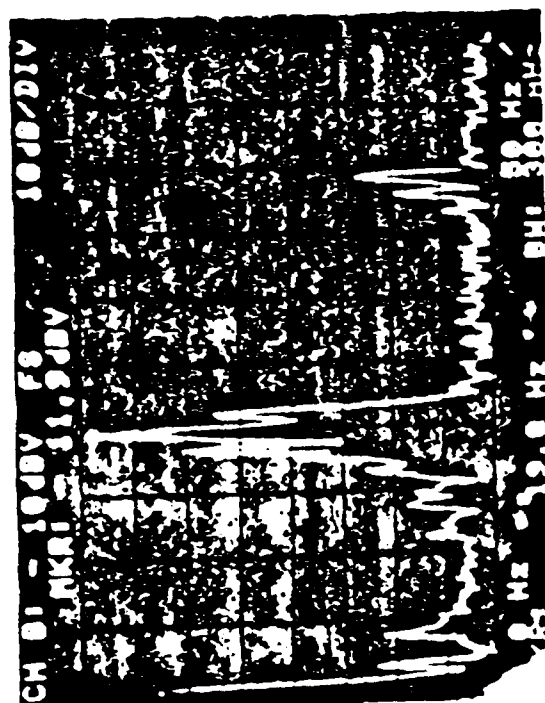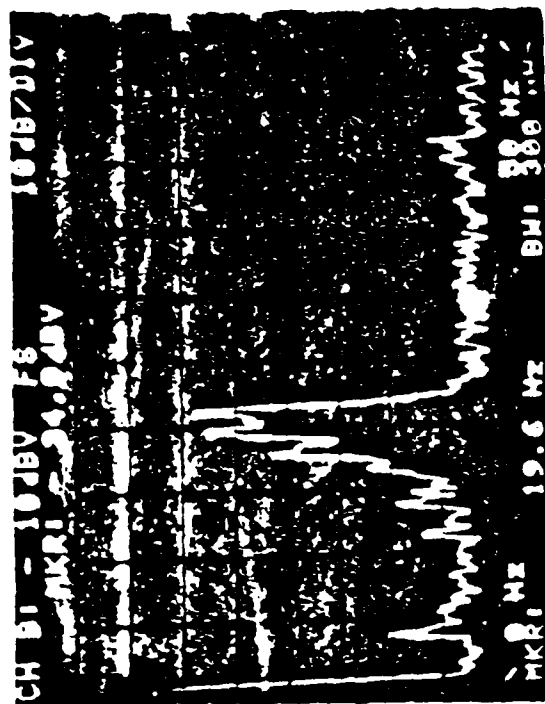The Q of the accelerometer is given by

FIG.5.2. The Experimental Setup

$$Q = \frac{\omega_0}{\dfrac{B_1}{m_1} + \dfrac{G}{m_2}} \tag{5.5}$$

where $\omega_0^2 = (\dfrac{K_1}{m_1})$. When the control gain G is increased, Q is reduced. Dependent on this concept, a control circuit is shown in Fig.5.2. The bandpass filter is made by cascading a high pass and a low-pass filter. This bandpass filter makes the gain higher at the resonant frequency and the gain lower elsewhere. This filter will limit the noise of the control circuit in the signal range. Figure 5.3 shows test results. The resonant frequency of 19.8 Hz was dropped about 20 db. From equation (5.5), Q can be reduced to 1. But here it is lowered about 20db. The reason is that the gradiometer consists of two accelerometers. They have resonant frequencies which differ only a little and they are out of phase with each other. Therefore, after 19.8 Hz is lowered the other resonance peak will be driven if the gain and phase are right. But the electromechanical damping cannot give us more attenuation in this special structure. We need to find some other way. The next section will discuss a electronic damping method.

5.3. Electronic Damping [Wang,1979]

A mass-spring accelerometer, as shown in Fig.5.1 can be represented by an LCR circuit as shown in Fig.5.4. If we have some ways to increase the resistance R, the Q of the LC circuit will be reduced. A simple block diagram is shown in Fig.5.5. An additional electronic resistor is introduced by

Fig.5.3. The Test Result of the Mechanical Cool Damping

a. The Output of the Gradiometer with the Feedback Loop Open

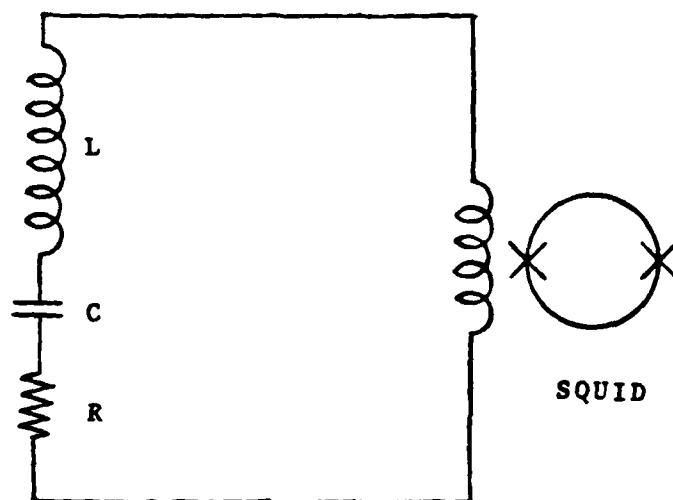b. The Output of the Gradiometer with the Feedback

Loop Closed

Fig.5.4.The equivalent circuit of Fig.5.1

FIG.5.5. A Cool Damping Block Diagram for an Equivalent RLC
Accelerameter[Wang,1979]

$\dfrac{V_f(S)}{I(S)}$ in the signal pickup loop. The new Q factor is

$R + \dfrac{V_f(S)}{I(S)}$. If we can control $\dfrac{V_f(S)}{I(S)}$, we can control the Q of the LCR circuit. In Fig.5.5 the electronic resistance is given by

$$\frac{V_f(S)}{V_s(S)} = GH(S) = R_e \qquad . \qquad (5.6)$$

Because we are only interested in the behavior at the resonance, $H(S)$ can be a bandpass filter, as $H(S) \dfrac{CS}{S^2 + AS + B}$ which has a high gain at the resonance frequency. When the gain G, in equation (5.6), is increased, the resistance R is increased and the Q of the RLC circuit is decreased. The actual block digram is shown in Fig.2.15 from V_{in} to V_1. This bandpass filter has a 50db difference in the frequency range from 0.5 Hz to 20 Hz. The test results are shown in Fig.5.7. The resonant frequency 19.6 Hz is dropped about 40db.

5.4.Minimum Q Achievable [Wang,1979;Mapoles,1980]

From equation (5.6), R_e may be as large as we want by increasing the gain of the feedback path. Thus it would seem that the Q of the accelerometer can be made as low as desired. This is not quite possible in practice, since the current induced by $V_f(S)$ in the input of the SQUID in Fig.5.5 is not considered in this model. Actually the current detected by the SQUID is the difference of the

Fig.5.6. A Block Diagram of Electronic Cool Damp for an Accelerometer where M is the Mutual Inductance between L and L_2

signal and the induced feedback current. The block diagram of the closed-loop feedback is shown in Fig.5.8 where $\frac{M}{S}$ is due to the transformer associated with L and L_2, N is defined by $\frac{I(S)}{I_f(S)} = \frac{M}{L_1 + L_2}$; G is the control gain; M is the mutual inductance between L and L_2. Solving the closed-loop equation, the feedback voltage is

$$V_f(S) = \frac{GS}{S + \frac{GN}{M}} I(S) \quad . \tag{5.7}$$

The impedance seen by the input circuit at the resonant frequency is

$$Z_f(S_0) = \frac{V_f(S_0)}{I(S_0)} = \frac{MaS_0}{N(S_0 + a)} \tag{5.8}$$

where $a = \frac{NG}{M}$. Substituting $j\omega_0$ for S_0, the impedance is

$$Z_f(j\omega_0) = \frac{a\omega_0^2 + ja\omega_0}{\omega_0^2 + a^2} \quad . \tag{5.9}$$

The real part of $Z_f(j\omega_0)$ is the equivalent resistor. The imaginary part of $Z_f(j\omega_0)$ is positive and increases the inductance of the resonating circuit. They are

$$R_e = \frac{a\omega_0^2}{\omega_0^2 + a^2} \quad ; \tag{5.10}$$

$$L_e = \frac{a^2\omega_0^2}{\omega_0^2 + a^2} \quad . \tag{5.11}$$

When the feedback gain G is varied, the parameter a is

varied too. The resistance R attains a maximum at $a = \omega_0$.

$$R_e\big|_{a = \omega_0} = \frac{M\omega_0}{2N} \qquad . \tag{5.12}$$

The resistive feedback will increase energy dissipation while the inductive feedback will *pump energy back* into the system. The system's Q will be minimum when these two are balanced.

The minimum Q is about 10 as calculated by Evan R. Mapoles [Maooles,1981]. In my experiment, the resonance peak is reduced about 40db; therefore, the minimum Q is about 500. The reason mine is larger than Mapoles is that I feedback the output of the SQUID amplifier to the SQUID itself directly so the loop gain is limited otherwise the additional input signal will overload the SQUID.

5.5. Discussion of Results

This chapter tests two different ways to reduce the Q of an accelerometer at low temperature. There are some adventages and disadventages in these methods. In the electromechanical method, as introduced in section 5.2, the Q of the superconducting accelerometer tends to zero theoretically which is shown in equation (5.5). But, in practice, due to the different spring modes associated with the accelerometers, the reduction Q of the accelerometer is limited by driving up different spring modes in this system, in which, while the resonant peak is reduced, the other new peak will go up. If we have a very narrow bandpass filter

without phase changing in the feedback loop, for example, only a single frequency can go through this filter, then the expression of Q is just like equation (5.5), and the Q of this system, shown in Fig.5.2, will drop to zero. The major disadventage of this method is the gradiometer has to be soft mounted, otherwise, the current-force converter cannot work.

In contradistinction to the above discussion, the gradiometer with electrical Q damping can be hard mounted. This is a very attractive feature because the size of the whole set will be much simplified. It is possible to put this gradiometer in the space shuttle bus to test the gravity of the earth. Due to feedback inductance into the signal pickup loop, the Q of the accelerometer cannot tend to one. If we need to reduce the Q of the accelerometer to one, a special filter is needed in which the filter has a pole at the right side of the S plane. Those special filters will be discussed in the next chapter.
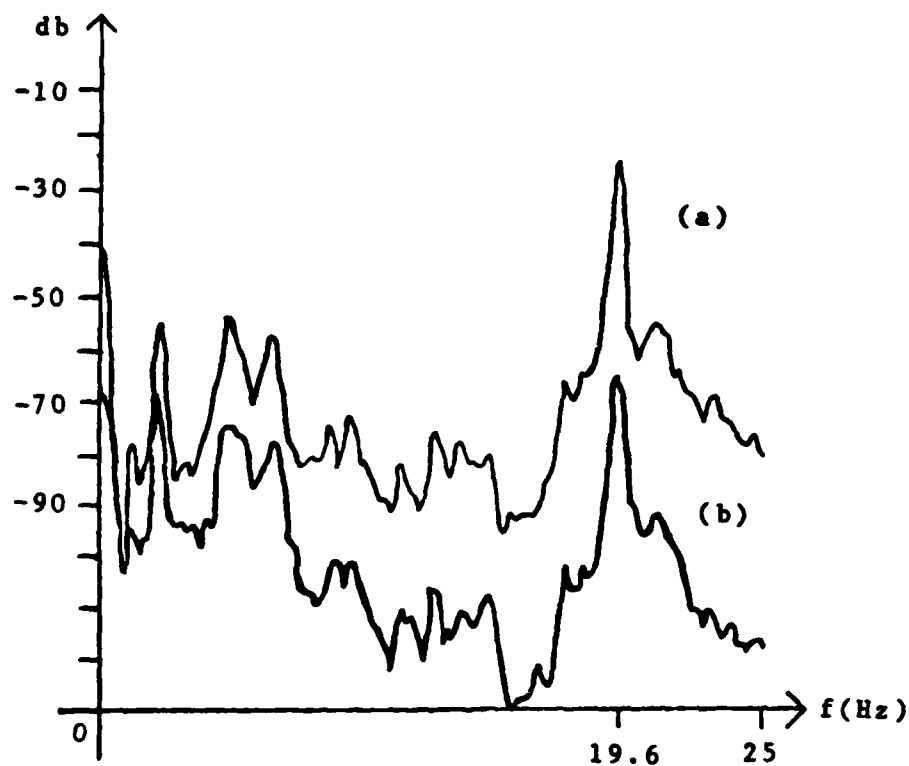
Fig.5.7. The Test Result of the Electronic Cool Damping

a. The Output of the Gradiometer with the Feedback Loop Open

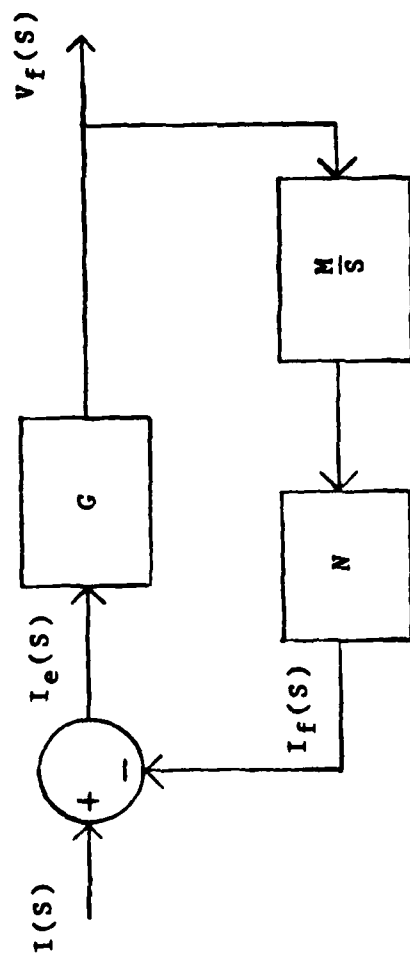b. The Output of the Gradiometer with the Feedback Loop
   closed

Fig.5.8. The Block Diagram of the Closed-loop Feedback Circuit. The bandpass filter which is shown in Fig.5.6 is omited when only resonant frequency is considered

CHAPTER 6

DISCUSSION AND OPEN PROBLEMS

We have studied different mass-spring systems. The primary results demonstrate that the performance of these systems is very close to the expected behavior, although some problems remain to be solved.

In the wide band superspring experiment, the overall gain G is given by (see equation (1.7))

$$G = 1 - \frac{\omega_1^2}{\omega_0^2} \qquad (6.1)$$

Where ω_0 is the open loop resonant frequency and ω_1 is the closed loop resonant frequency. When $\omega_0 = 6.4 Hz$ and $\omega_1 = 1.2 Hz$, we get $G = 0.965$. Therefore the acceleration of m_1, which is due to the pressure of m_2, has been cancelled by about 96.5% by the feedback. In order to make $G = 1$, some special amplitude control circuit is needed. Let us recall equation (1.4) here;

$$X_2 - X_1 = \frac{s^2 X_2}{\dfrac{B_1}{m_1} s + \dfrac{K_1}{m_1}} \qquad . \qquad (6.2)$$

After closing the feedback loop, equation (6.2) becomes

$$X_2 - X_1 = \frac{s^2 X_2}{\dfrac{B_1}{m_1} s + (1 - G)\dfrac{K_1}{m_1}} \qquad . \qquad (6.3)$$

Assuming B_1 is very small the amplitude $X_2 - X_1$ is

$$|X_2 - X_1| = \frac{\omega^2 X_2}{(1 - G)\dfrac{K_1}{m_1}} \quad .$$ (6.3)

When $(1 - G)\dfrac{K_1}{m_1}$ tends to zero $X_2 - X_1$ will be infinite

Therefore an amplitude control circuit is necessary to use

in future designs.

In the electromechanical Q reduction experiment of Chapter 5, a special single frequency bandpass filter is mentioned. By using this kind of filter, it is possible to cut down on very resonant peaks. A prototype filter's block diagram is shown in Fig.6.1. After the phase lock loop locks on one resonance frequency of interest, the VCO outputs a sine wave with the same phase as the locked resonance frequency. The second phase detector outputs an amplitude for the resonance. Then these two signals are multiplied to give a single frequency which has the same phase and amplitude as the resonance frequency of interest.

In the electrical Q reduction experiment, we found the minimum value of Q in Chapter 5. In order to reduce Q more let us look at Fig.5.8. again and insert a filter $H(S)$ in the main path. The transfer function is given by

$$\frac{V_f(S)}{I_s(S)} = \frac{SGH(S)}{S + GNMH(S)} \quad .$$ (6.4)

In order to get $Q = 1$, $\dfrac{V_f(S)}{I_s(S)}$ has to be a resistive

constant.   Now   let $\dfrac{V_f(S)}{I_s(S)} = R_e$.   We can find that

$$H(S) = \frac{R_e S}{SG - GNMR_e} \qquad\qquad (6.5)$$

This   transfer   function   has   a   pole   in   the   right   half   S
plane.   It   is   an   unstable   system.   If   we   can   find   some
special   way   to   realize   this   transfer   function,   for   example
by   a   digital   network,   we   will   reduce   Q   to   1   and   the
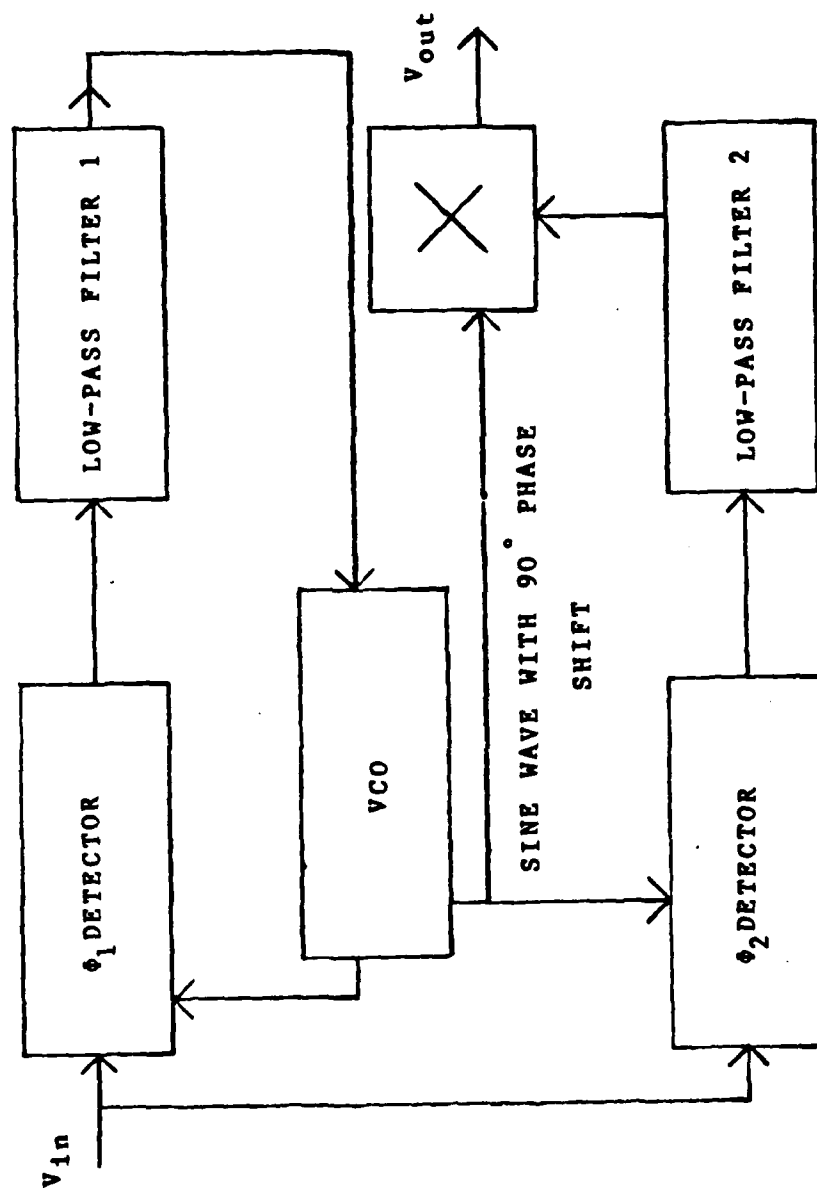sensitivity will be tremendously increased.

Fig.6.1. The Block Diagram of a Single Frequency Filter.

APPENDIX A

THE MOTION OF A DOUBLE MASS-SPRING SYSTEM

The structure of a double mass-spring system is shown in Fig.A.1, where K_1 and K_2 are the spring constants; B_1 and B_2 are the damping factors of these springs; X_1, X_2 and X_3 are the absolute displacement; and f_b is the additional driving force which is from a control system. In the time domain, the equation of motion for m_2 due to m_3 and m_1 is

$$\ddot{X}_2 m_2 + B_2(\dot{X}_2 - \dot{X}_3) + K_2(X_2 - X_3) + B_1(\dot{X}_2 - \dot{X}_1)$$

$$K_1(X_2 - X_1) = 0 \tag{A.1}$$

where $f_b = 0$ for the time being; the dot is a symbol of differentiation. In the Laplace transform S domain, equation (A.1) becomes

$$m_2 X_2 S^2 + B_2(X_2 - X_3)S + K_2(X_2 - X_3) + B_1(X_2 - X_1)S$$

$$+ K_1(X_2 - X_1) = 0 \tag{A.2}$$

which is

$$(m_2 S^2 + B_2 S + K_2)X_2 + B_1(X_2 - X_1)S + K_1(X_2 - X_1)$$

$$= (B_2 S + K_2)X_3 \quad . \tag{A.3}$$

The equation of motion of m_1 due to m_2 is

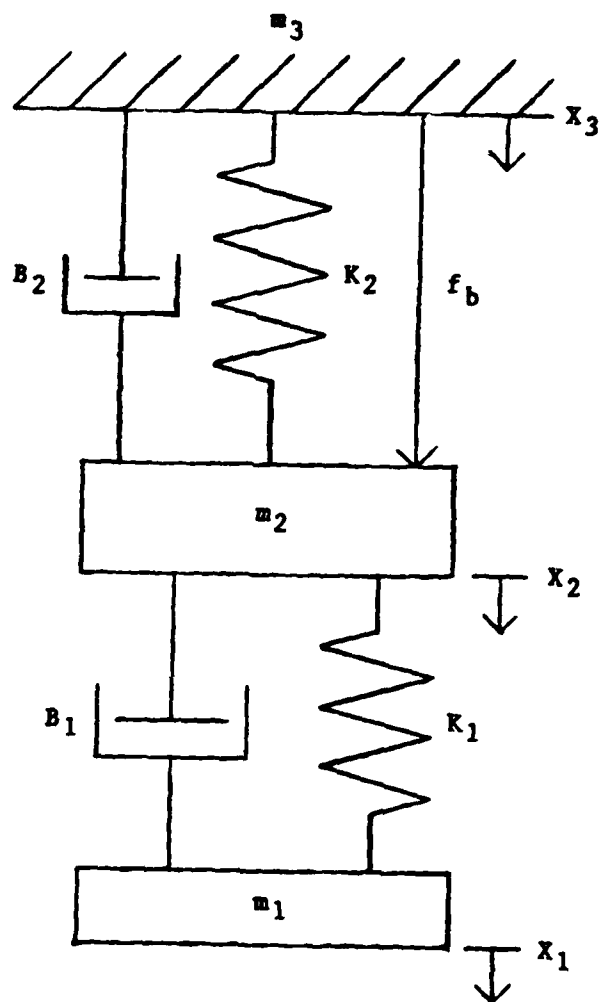$$\ddot{X}m_1 + B_1(\dot{X}_1 - \dot{X}_2) + K_1(X_1 - X_2) = 0 \quad . \tag{A.4}$$

Fig.A.1. A Schamatic of a Double Mass-spring System

In the S domain, the equation (A.4) becomes

$$m_1 X_1 S^2 + B_1 (X_1 - X_2)S + K_1 (X_1 - X_2) = 0 \qquad (A.5)$$

which is

$$X_2 - X_1 = \frac{X_2 S^2}{S^2 + \frac{B_1}{m_1}S + \frac{K_1}{m_1}} \qquad . \qquad (A.6)$$

Substituting (A.6) into (A.3), we get

$$X_2 - X_1 = \frac{(\frac{B_2}{m_2}S + \frac{K_2}{m_2})S^2 X_3}{(S^2 + \frac{B_2}{m_2}S + \frac{K_2}{m_2})(S^2 + \frac{B_1}{m_1}S + \frac{K_1}{m_1}) + \frac{B_1}{m_2}S^3 + \frac{K_1}{m_2}S^2} \qquad (A.7)$$

In the denominator, we can omit $\frac{B_1}{m_2}S^3 + \frac{K_1}{m_2}S^2$ terms because

they only shift the two resonances of $\omega_2^2 = \frac{K_2}{m_2}$ and $\omega_1^2 = \frac{K_1}{m_1}$ a

little.   They   will   not   affect   the   transfer   function.

Therefore, we replace equation (A.7) by

$$X_2 - X_1 = \frac{(\frac{B_2}{m_2}S + \frac{K_2}{m_2})S^2 X_3}{(S^2 + \frac{B_2}{m_2}S + \frac{K_2}{m_2})(S^2 + \frac{B_1}{m_1}S + \frac{K_1}{m_1})} \qquad . \qquad (A.8)$$

Substituting (A.6) into (A.8) we get

$$X_2 = \frac{(\frac{B_2}{m_2}S + \frac{K_2}{m_2})X_3}{S^2 + \frac{B_2}{m_2}S + \frac{K_2}{m_2}} \qquad (A.9)$$

or

$$X_2 = \frac{(\frac{\omega_2}{Q_2}S + \omega_2^2)X_3}{S^2 + \frac{\omega_2}{Q_2}S + \omega_2^2} \qquad (A.10)$$

where $\frac{B_2}{m_2} = \frac{\omega_2}{Q_2}$ and $\frac{K_2}{m_2} = \omega_2^2$.   In   the   Bode   plot, equation (A.10) is represented by Fig.A.2.

From equation (A.4), we get

$$X_2 - X_1 = \frac{X_1 S^2}{\frac{B_1}{m_1}S + \frac{K_1}{m_1}} \qquad . \qquad (A.11)$$

Substituting equation (A.11) into equation (A.8) we get

$$X_1 = \frac{(\frac{B_2}{m_2}S + \frac{K_2}{m_2})(\frac{B_1}{m_1}S + \frac{K_1}{m_1})X_3}{(S^2 + \frac{B_2}{m_2}S + \frac{K_2}{m_2})(S^2 + \frac{B_1}{m_1}S + \frac{K_1}{m_1})} \qquad (A.12)$$

or

$$X_1 = \frac{(\frac{\omega_2}{Q_2}S + \omega_2^2)(\frac{\omega_1}{Q_1}S + \omega_1^2)X_3}{(S^2 + \frac{\omega_2}{Q_2} + \omega_2^2)(S^2 + \frac{\omega_1}{Q_1}S + \omega_1^2)} \qquad (A.13)$$

where $\frac{B_2}{m_2} = \frac{\omega_2}{Q_2}$; $\frac{K_2}{m_2} = \omega_2^2$; $\frac{B_1}{m_1} = \frac{\omega_1}{Q}$ and $\frac{K_1}{m_1} = \omega_1^2$.   In   the   Bode plot, equation (A.13) is represented in Fig.A.3.
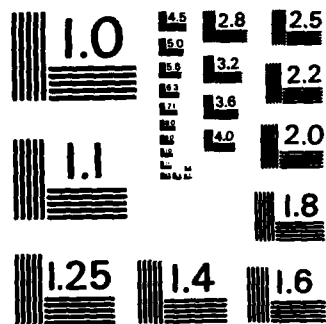
END

FILMED

DTIC

MICROCOPY RESOLUTION TEST CHART
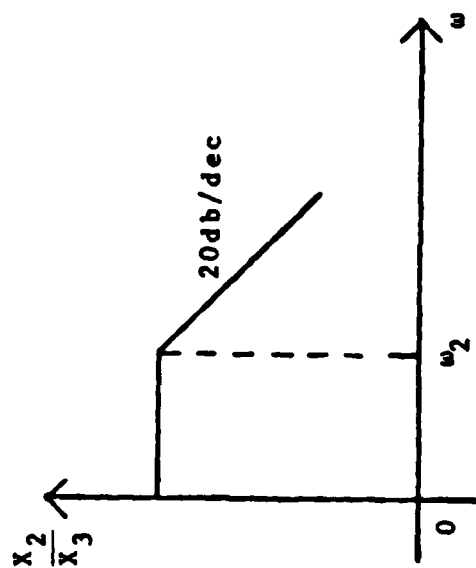
NATIONAL BUREAU OF STANDARDS-1963-A
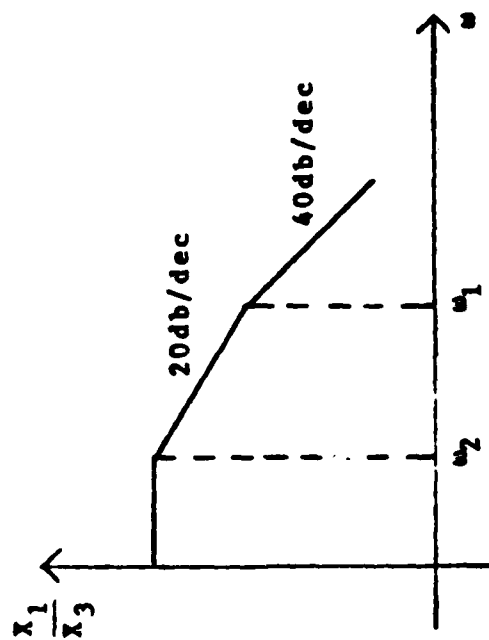
Fig.A.2. The Bode Plot of Equation (A.10)

Fig.A.3. The Bode Plot of Equation (A.13)

APPENDIX B

THE MOTION OF AN ACTIVE DOUBLE MASS-SPRING SYSTEM

Now let us set, in Fig.A.1., f_b to equal $GH(S)(X_2 - X_1)$, where G is the control gain and $H(S)$ is the frequency compensation function if any. The new equation of the motion is

$$m_2 X_2 S^2 + B_2(X_2 - X_3)S + K_2(X_2 - X_3) + B_1(X_2 - X_1)$$

$$+ K_1(X_2 - X_1) + GH(S)(X_2 - X_1) = 0 \quad . \quad (B.1)$$

In the ideal situation, we can omit $B_1(X_2 - X_1)S + K_1(X_2 - X_1)$. We get

$$m_2 X_2 S^2 + B_2(X_2 - X_3)S + K_2(X_2 - X_3)$$

$$+ GH(S)(X_2 - X_1) = 0 \quad . \quad (B.2)$$

By substituting equation (A.6) into (B.2), we get

$$X_2 - X_1 = \frac{(\frac{B_2}{m_2}S + \frac{K_2}{m_2})S^2 X_3}{(S^2 + \frac{B_2}{m_2}S + \frac{K_2}{m_2})(S^2 + \frac{B_1}{m_1}S + \frac{K_1}{m_1}) + S^2 \frac{GH(S)}{m_2}} \quad . \quad (B.3)$$

By substituting equation (A.6) into (B.3), we get

$$X_2 = \frac{(\frac{B_2}{m_2}S + \frac{K_2}{m_2})(S^2 + \frac{B_1}{m_1}S + \frac{K_1}{m_1})X_3}{(S^2 + \frac{B_2}{m_2}S + \frac{K_2}{m_2})(S^2 + \frac{B_1}{m_1}S + \frac{B_1}{m_1}) + S^2 \frac{GH(S)}{m_2}} \quad . \quad (B.4)$$

By substituting equation (A.11) into (B.3), we get

$$X_1 = \frac{(\frac{B_2}{m_2}S + \frac{K_2}{m_2})(\frac{B_1}{m_1}S + \frac{K_1}{m_1})X_3}{(S^2 + \frac{B_2}{m_2}S + \frac{K_2}{m_2})(S^2 + \frac{B_1}{m_1}S + \frac{K_1}{m_1}) + S^2\frac{GH(S)}{m_2}} \quad . \quad (B.5)$$

Now, we look at equation (B.4) in detail. By rearranging equation (B.4), we find

$$X_2 = \frac{(\frac{B_2}{m_2}S + \frac{K_2}{m_2})X_3}{(S^2 + \frac{B_2}{m_2}S + \frac{K_2}{m_2}) + \frac{S^2 GH(S)/m_2}{S^2 + SB_1/m_1 + K_1/m_1}} \quad . \quad (B.6)$$

When the frequency ω is lower than $\omega_1^2 = (\frac{K_1}{m_1})$, equation (B.6) can be written as following:

$$X_2 \doteq \frac{(\frac{B_2}{m_2}S + \frac{K_2}{m_2})X_3}{(S^2 + \frac{B_2}{m_2}S + \frac{K_2}{m_2}) + \frac{S^2 GH(S)}{m_2}}$$

$$= \frac{\frac{X_3(SB_2/m_2 + K_2/m_2)}{(1 + GH(S)/m_2)}}{S^2 + \frac{SB_2/m_2}{1 + GH(S)/m_2} + \frac{K_2/m_2}{1 + GH(S)/m_2}} \quad . \quad (B.7)$$

The new resonance frequency is given by $\omega_n^2 = \dfrac{\frac{K_2}{m_2}}{1 + \frac{GH(S)}{m_2}}$.

When the frequency ω is highter than $\omega_1^2 = (\frac{K_1}{m_1})$, in equation (B.6), the equation (B.6) can be writen as following:

$$X_2 \doteq \frac{(\frac{B_2}{m_2}S + \frac{K_2}{m_2})X_3}{S^2 + \frac{B_2}{m_2}S + \frac{K_2}{m_2}} \qquad . \qquad\qquad (B.8)$$

By the same analysis method, from equation (B.5), we find

$$X_1 = \frac{(\frac{B_2}{m_2}S + \frac{K_2}{m_2})(\frac{B_1}{m_1}S + \frac{K_1}{m_1})X_3}{(S^2 + \frac{B_2}{m_2}S + \frac{K_2}{m_2})(S^2 + \frac{B_1}{m_1}S + \frac{K_1}{m_1} + \frac{S^2 GH(S)}{m_2})} \qquad \omega < \omega_1 \quad (B.9a)$$

$$X_1 = \frac{(\frac{B_2}{m_2}S + \frac{K_2}{m_2})(\frac{B_1}{m_1}S + \frac{K_1}{m_1})X_3}{(S^2 + \frac{B_2}{m_2}S + \frac{K_2}{m_2})(S^2 + \frac{B_1}{m_1}S + \frac{K_1}{m_1})} \qquad \omega > \omega_1 \quad (B.9b)$$

$$\text{where} \quad \omega_1^2 = \frac{K_1}{m_1} \quad ; \quad \omega_n^2 = \frac{\frac{K_1}{m_1}}{1 + \frac{GH(S)}{m_2}} \qquad .$$

APPENDIX C

POLE AND ZERO ANALYSIS OF ACTIVE MASS-SPRING SYSTEM

The appendices A and B are represented here by mathematical analysis. In this appendix, the root-locus method is used to analyse the equations shomn in appendices A and B. This will give us a very clear picture of the overall performance of a mass-spring system, specially, after changing gain of the loop or some parameter of the equations.

In the double mass-spring, from equation (B.4), the root-locus diagram is represented in Fig.C.1 by setting the denominator of equation (B.4) equal to zero where $\omega_2^2 = (\frac{K_2}{m_2})$ and $\omega_1^2 = (\frac{B_1}{m_1})$. Because the poles are always at the left side of the diagram, this system is always stable. The only trouble is that the Q of the ω_1 factor becomes higher and higher when the loop gain is increasing. From Fig.C.1 you can see that P_1 towards infinity of the imaginary axis after the loop gain is increased. In other words, the real part of P_1 is fixed and the imaginary part is increased. Then the system will be uncontrolable and this system will lose the feature of a low-pass filter. Consequently, a special compensation network is necessary to control the Q of ω_1. By setting $H(S) = \frac{1 + AS}{S^2 + BS + C}$ and choosing appropriate A, B and C, the root-locus diagram of the results is shown in Fig.C.2 where P_e and z_e are from A, B and C. In this new system, P_1 and P_2 both tend toward zero frequency. The new peak is caused

by P_e which comes from the compensation network. The P_e is not in the mass-spring system, so this system will not see this peak. In this method, the key point is to make a frequency compensation network. However, it is not easy to find and its adjustment is very complicated[Rinker III,1983].
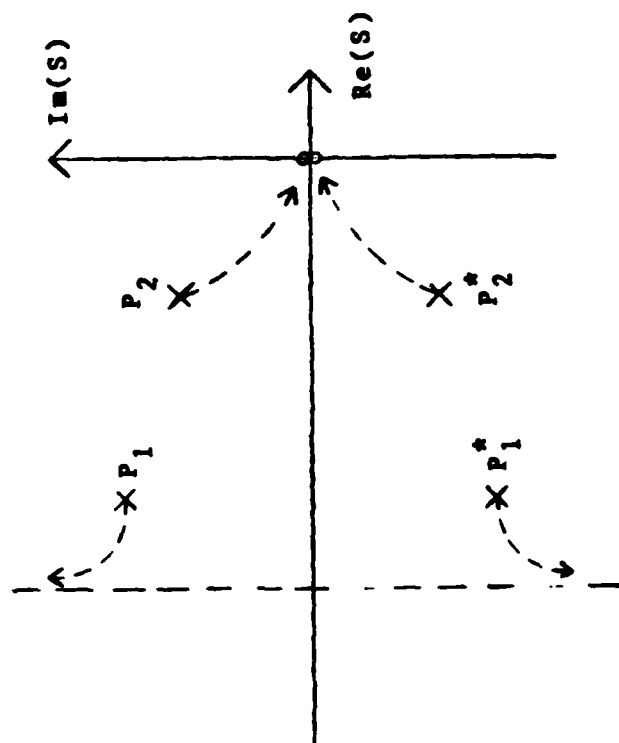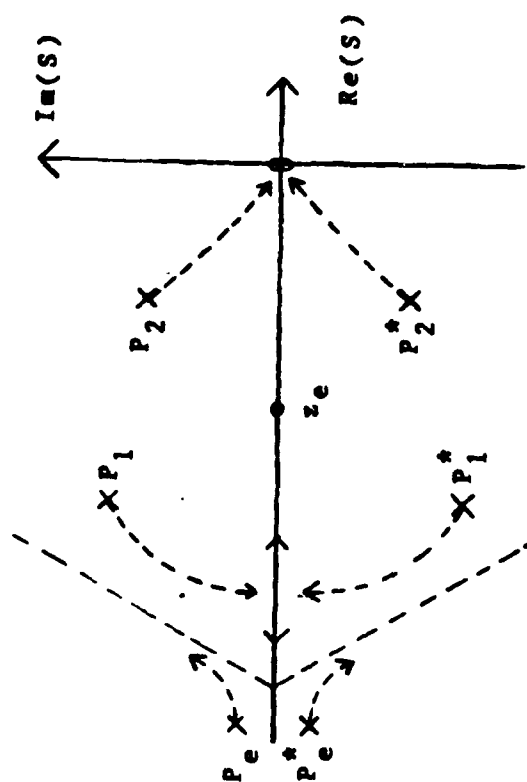
Fig.C.l.The Root-locus Diagram for Equation (B.4)

Fig.C.2.   The   Root-locus   Diagram   after   Frequency
            Compensation

APPENDIX D

THEORY OF THE SQUID [Lounasmaa,1974]

The operation of the SQUID is based on London's (1950) concept of fluxoid quantization in a superconductor and on Josephson (1962,1951) tunneling through a "weak link" between two superconductors. The SQUID can be used for measurment of magnetic flux with an unprecedented sensitivity aproaching 0.1×10^{-18}Wb (10^{-11}gauss cm^2).

Figure D.1 is a schematic illustration of a dc-SQUID, consisting of a superconducting ring, with two extensions and two Josephson junctions (weak links). The Josephson junctions are weakly superconducting. The current which just makes the Josephson junction operation normal is the critical current of this junction. When the external current J has been increased to its critical value J_c, a voltage suddenly appears across the Josephpson junction. A curve representing the transfer function of the superconducting ring when an external current J goes through the ring is shown in Fig.D.2. The critical current is not a constant. It will change when the flux in the ring is changed. Figure D.3 shows the relationship between the critical current and the external flux where ϕ_0 is the quantam flux. Now let us combine Fig.D.2 and Fig.D.3. Doing this we can find the transfer function between the voltage across the Josephson junction and the external applied flux. This relationships is illustrated in Fig.D.4.

For a bias current J_0 in Fig.D.4., when the external

flux changes by only $\frac{1}{2} \phi_0$, the SQUID has a big voltage $V_2 - V_1$ output. The sensitivity of a SQUID is about $10mV/pWb$ ($10^6 V/Wb$). A typical circuit of a SQUID amplifier is shown in Fig.D.5[Lounasmaa,1974].

J

EXTENSION

+

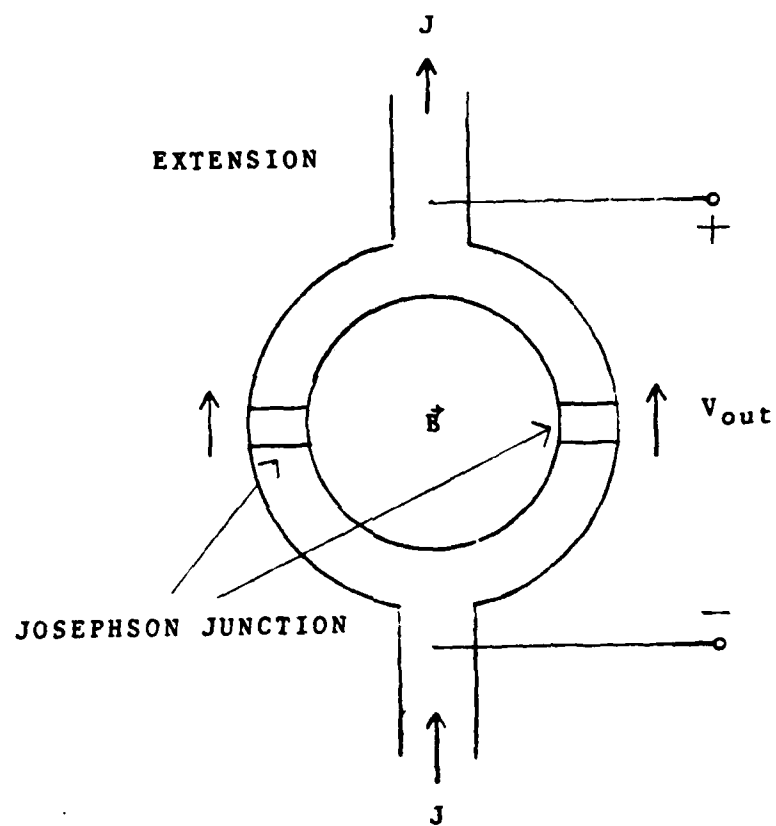$\vec{B}$

V_{out}

JOSEPHSON JUNCTION

J
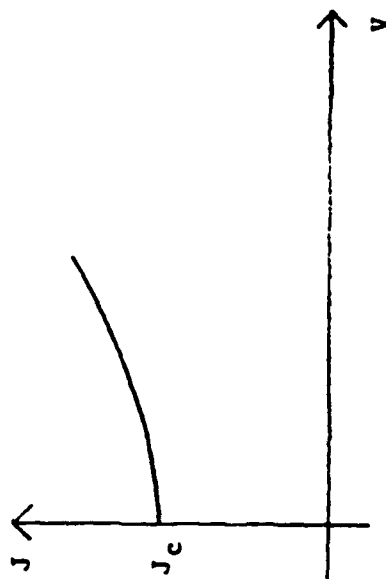
Fig.D.1. Schematic Illustration of a dc-SQUID

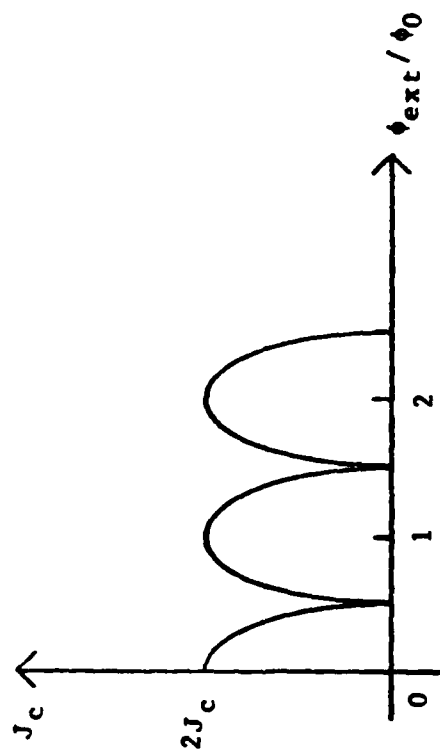Fig.D.2. The Current-voltage Transfer Function of a Superconducting Ring

Fig.D.3. The Critical Current of a dc-SQUID as a Function of the Externally Applied Magnetic Flux
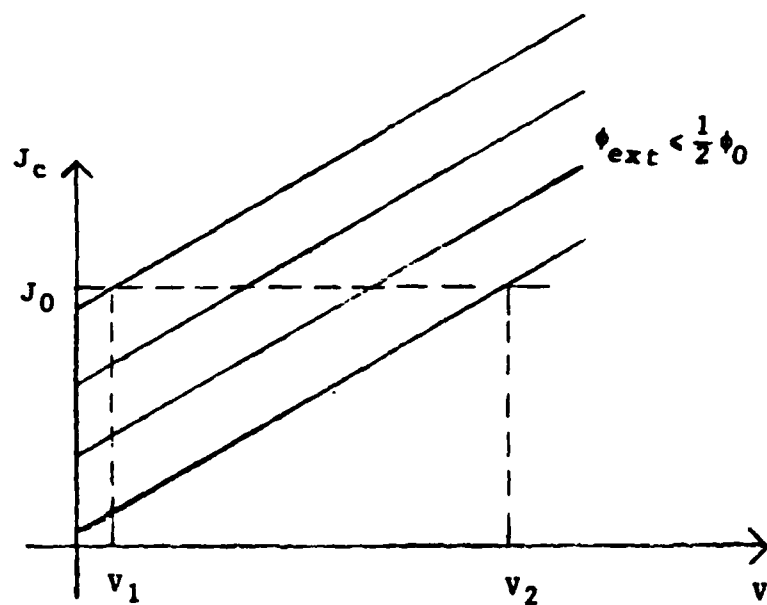
Fig.D.4.The Transfer Function from ϕ_{ext} to V across
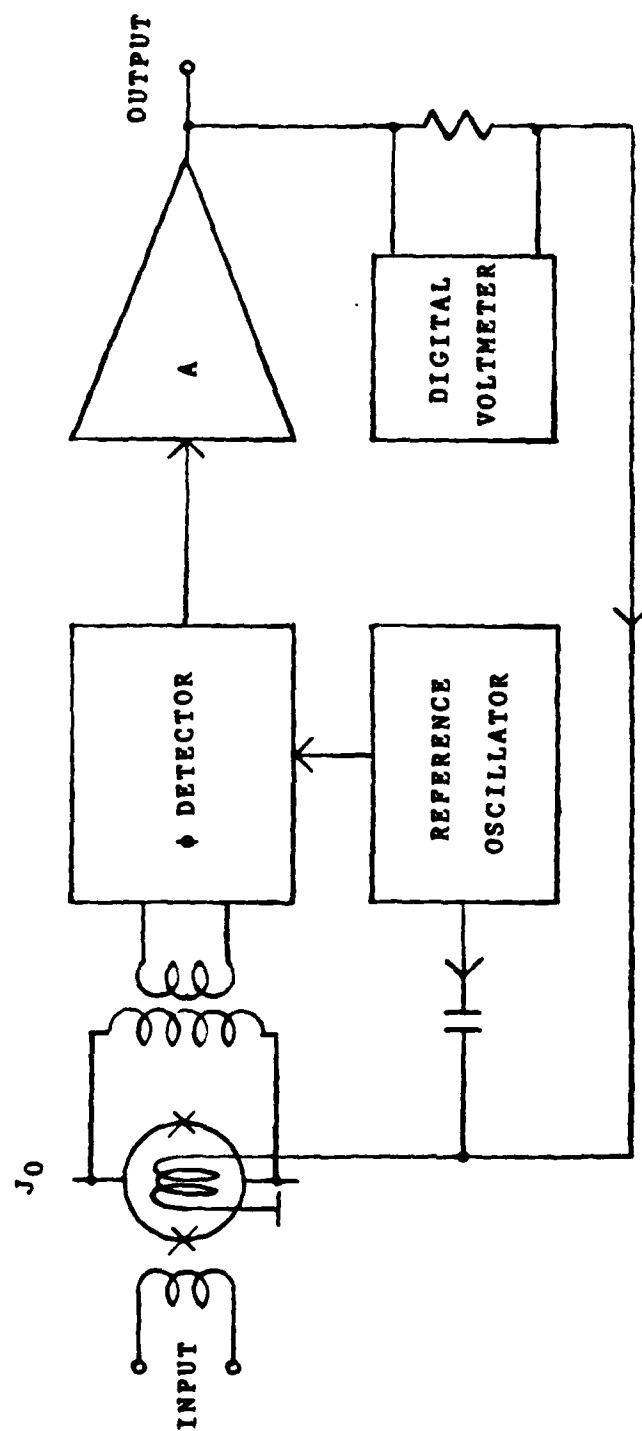the Josephson Junction

FIG.D.5. A BLOCK DIAGRAM OF A SQUID AMPLIFIER

REFERENCE

Chan, Hinghung Authony, "Null Test of the Gravitational
Inverse Square Law with a Superconducting Grafity
Gradiometer", Ph.D. thesis, University of of Maryland
Dep. of Physiscs and Astronomy (1982).

Chen,Jeng-Heng, "Helium Thrustor Propulsion System for
Precise Attitude Control and Drag Compensation of the
Gravity Prob-B Satellite", Ph.D. thesis, Stanford
University, Dep. of Physics(1983).

Linsay, Paul S. and David H. Shoemaker, "Low-noise RF
Capacitance Bridge Transduce", Rev. Sci. Instrum, 53(7)
P.1014-1019 July (1982).

Lounasmaa, O. V., Experimental Principles and Methods
Below 1K, Academic Press, New York, (1974).

Moodl, M. Vol, et al, IEEE Trans. Mag. MAG-19, 461 (1983)

Moody, M. Vol, Personal Conversation (1984).

Paik, Ho Jung, "Analysis and Development of a Very Sensitive
Low Temperature Gravitational Radiation Detector",
Ph.D. thesis, Stanford University, Dep. of Physics
(1974).

Rinker III, Robert Lee, "Super Spring--A New Type of Low-
Frequency Vibration Isolation", Ph.D. thesis,
University of Colorado, Dep. of Physics (1983).

Sileconix Inc., Small Signal FET Design Catalog (1983).

Wang, Kai Yuen, "Modeling and Error Analysis of a
Superconducting Gravity Gradiometer", Ph.D. thesis,
Stanford University, Dep. of Physics (1979).

Weinstoch, Herbert, "Design of a Percision Tilt and
Vibration Isolation System", NASA Technical Report,
Electronics Research Center, Cambridge Mass. (1968).

END

FILMED

12-85

DTIC